following examination. This group of patients had never received embryo transfers. Patients were excluded who had uterine endometrial irregularity including endometrial polyp or submucosal myoma, amenorrhea because of premature ovarian insufficiency, or were over 43 years of age. Clinical data were analyzed by chi-square test and residual analysis. $P < 0.05$ was considered to be statistically significantly different. Informed consent was provided by all patients for this study.

Patient samples were collected at the mid luteal phase, the fifth to seventh day post-ovulation, which is considered to be an implantation window[48]. An 8-Fr Foley catheter connected to the disposable 5-ml syringe (TERUMO) was inserted into the uterine cavity through the cervix. Five milliliters of saline (Otsuka Pharmaceutical) was then injected into the cavity, immediately aspirated without contamination by the vaginal and cervical fluids, and collected in eppendorf tubes. The collected uterine flushing was centrifuged at 1500 *g* for 10 min at room temperature to remove blood corpuscles, exfoliated epithelial cells and large protein complexes. The supernatants were then transferred to new eppendorf tubes, heated for inactivation of endogenous proteases, and then stored at −20°C until use. The protein concentration of each sample was measured by the Biuret test[49]. Samples (50 μl) of human or mouse uterine secretions (as detailed below) were boiled at 95°C for 10 min in 50 μl Laemmli's SDS sample buffer containing 2% SDS, 62.5 mM Tris-HCl (pH 6.8), 0.005% bromophenol blue, and 7% glycerol. Then, 10 μl samples were resolved by SDS-polyacrylamide gel electrophoresis on 10% acrylamide gels and then transferred to Immobilon-FC (Millipore). Detection of immune complexes formed by proteins of interest and primary antibodies was performed by enzyme-linked color development with horseradish peroxidase conjugated to secondary antibodies. The intensity of the band was quantified using NIH Image J software. Briefly, the signal was outlined and the mean intensity and background fluorescence were measured. The specific signal was calculated by dividing the band intensities for CD9 by those for actin. If the relative band intensitiy for CD9 was less than 0.01, the sample was considered as "CD9 negative" in this study.

This study was approved by the Ethics Committee at the Japanese Institution for Standardizing Assisted Reproductive Technology (#11-09). Samples were collected only from patients who had provided informed consent.

Animals. Eight- to 12-week-old female C57BL/6N mice and male B6C3F1 mice, a cross between female C57BL/6N and male C3H mice, were purchased from SLC (Shizuoka, Japan).

Cd9$^{-/-}$ mice were generated as described previously[13], and backcrossed with a C57BL/6N genetic background. *Cd9*$^{-/-}$ mice expressing CD9 tagged at the N-terminus with GFP (CD9-GFP) (*Cd9*$^{-/-}$*TG*) were generated as described previously[16]. The construct carrying mouse CD9 tagged at the C-terminus with GFP (CD9-GFP) was sub-cloned into plasmid DNA containing the mouse ZP3 promoter[50]. Transgenic mice with a *Cd9*$^{-/-}$ background were produced by crossmating with *Cd9*$^{-/-}$ mice. The genotypes of mice were determined by standard procedures as described previously[16].

All mice were housed under specific pathogen-free controlled conditions. Food and water were available *ad libitum*. The procedures for performing animal experiments were in accordance with the principles and guidelines of the Care and Use of Laboratory Animals at the National Research Institute for Child Health and Development. The animal committee of the National Research Institute for Child Health and Development approved the experiments including the use of live animals (Experimental number is 04-004).

Vaginal smear test and collection of mouse uterine secretions. *Cd9*$^{-/-}$*TG* and *Cd9*$^{+/+}$ female mice were examined by vaginal smear cytology and assigned to one of four phases of the estrous cycle as described previously[4] (Supplementary Fig. 1a). Briefly, a vaginal smear was collected with a moistened cotton swab, applied to a glass slide, stained with hematoxylin, and then observed under a stereomicroscope. According to the microscopic characteristics of the vaginal smear, the mice were classified as proestrus, estrus, metestrus, or diestrus. Because the uterus undergoes hormonal changes during the estrous cycle, and is distended at the estrus stage because of an increase of uterine secretions, we collected the uterine secretions from estrus-stage mice. Mice staged at estrus were sacrificed and their uteri were incised and flushed with 50 μl saline. Then, the flushed solution was collected from each of uterine horns and subjected to immunoblotting as described above.

Immunohistochemical analysis of mouse uterine tissues. Estrus-stage female mice were sacrificed and their uteri were excised and fixed with 4% paraformaldehyde for 3 h at 4°C. After fixation, the uterine tissues were immersed in a 30% sucrose solution at 4°C until they sank to the bottom of the tubes and then embedded in OCT (Tissue-Tek) and frozen at −80°C. The tissues were then sectioned at 10 μm with a cryostat (CryoStar NX70; Thermo Scientific). The sections were dried and incubated with primary antibodies (2.5 μg/ml) in HEPES-buffered saline (HBS; 10 mM HEPES (pH 8.0), 0.15 M NaCl, and 3% fetal bovine serum [FBS]) for 2 h at room temperature, and then Alexa Fluor 488- or 546-conjugated IgGs, followed by three washes in HBS. Nuclei were then counterstained with DAPI at a final concentration of 10 μg/ml in HBS for 30 min at room temperature, followed by three washes in HBS. Images were captured under a laser scanning confocal microscope (LSM 510 model; Carl Zeiss Microimaging, Thornwood, NY).

Wound healing assay. For the wound healing assay, three uteri each were harvested from sacrificed *Cd9*$^{-/-}$*TG* and *Cd9*$^{+/+}$ mice, and the endometrial epithelial cells were isolated by treatment with collagenase (WAKO Pure Chemical Industries) as described previously[51]. Briefly, uterine inner surfaces were treated with collagenase for 1 h at 37°C, and the uterine fluid was collected from intrauterine cavities. Then, the endometrial epithelial cells were centrifuged at 1,000 rpm for 10 min, washed with complete medium (Dulbecco's modified Eagles medium containing 20% FBS, 0.1 mg/ml heparin, 0.1 mg/ml endothelial cell mitogen [Biomedical Technologies], nonessential amino acids, sodium pyruvate, L-glutamine, and penicillin/streptomycin at standard concentrations), and cultured in fibronectin-coated tissue culture dishes (Asahi glass). Non-adherent cells were removed by changing the medium after 24 h.

After serum starvation, the confluent monolayer of epithelial cells was wounded lengthwise with a 200-μl pipette tip. Phase contrast images of the wounds were taken at 0, 3.5, and 17.5 h after the epithelial cells were injured at three random locations to examine the extent of wound closure using ImageJ software (National Institutes of Health, USA).

Immuno-electron microscopic analysis. Uterine secretions collected from *Cd9*$^{-/-}$*TG* and *Cd9*$^{+/+}$ female mice were incubated with an anti-CD9 mAb (0.5 μg/ml) at room temperature for 2 h and then 10 nm colloidal gold particles coupled to secondary antibodies at room temperature for 1 h. The samples were centrifuged at 12,000 rpm for 30 min at room temperature, and then the precipitates were washed three times with HBS. The precipitates were then fixed with glutaraldehyde and osmic acid solutions. Ultrathin sections were prepared as described previously[52].

Multiplex suspension array. Multiplex bead kits were purchased from the following manufacturers: LINCO Research (Kit a), Bio-Rad Laboratories (Kit b), R&D Systems (Kit c), and BioSource International (Kit d). The multiplex assay was performed to detect cytokines of interest in sextaplicate on two separate occasions according to the manufacturers' instructions. Standard curves for each cytokine using each kit were generated using the reference cytokine concentrations supplied by the manufacturers. Raw data (mean fluorescence intensity) from all kits were analyzed by MasterPlex Quantitation Software (MiraiBio) to obtain concentration values.

Repair of the endometrial epithelium by treatment with VEGF. To repair the endometrial epithelium damaged by parturition, VEGF was injected into the uterine cavity of *Cd9*$^{-/-}$*TG* female mice. To sustain the effect of VEGF in the uterine cavity, VEGF was covalently coupled to carboxylated microparticles (6 μm average diameter) (Polyscience). Briefly, 12.5 mg microparticles was suspended in 0.17 ml PolyLink Coupling Buffer containing 50 mM 2-(N-morpholino)ethanesulfonic acid (pH 5.2) and 0.05% Proclin-300. Twenty microliters of 200 mg/ml 1-ethyl-3-(3-dimethylaminopropyl)carbodiimide was added to the microparticle suspension. After gentle mixing, the microparticles were combined with 200 μg recombinant mouse VEGF (164 amino acid; R&D Systems) and incubated for 1 h at room temperature. After centrifugation for 10 min at 500 *g*, the microparticles were resuspended in 0.4 ml PolyLink Wash/Storage Buffer containing 10 mM Tris-HCl (pH 8.0), 0.05% bovine serum albumin (BSA), and 0.05% Proclin-300, and then stored at 4°C. Before VEGF injection, *Cd9*$^{-/-}$*TG* female mice were intercrossed with *Cd9*$^{-/-}$ male mice to deliver pups. At 1 week after parturition, mother mice were anesthetized with Avertin and their vaginas were filled with silicon using a 1-ml syringe attached to a 200-μl pipette tip, and the uterus was filled with VEGF-linked microparticles from backside lesions. Silicon (BECKMAN COULTER) was used to prevent VEGF-linked microparticles from leaking into the vagina and contaminating with BSA-linked microparticles in another uterine horn. At 7 days after microparticle injection, the mice were sacrificed and their uteri were examined histochemically by hematoxylin and eosin (H&E) staining. The rate of the repithelialization was calculated by (number of repithelialized site)/(total number of implantation site).

Statistical analysis. Comparisons were made using one-way analysis of variance following Scheffe's method, the Mann-Whitney U-test, or Fisher's exact test. Statistical significance was defined as $P < 0.05$. Results were expressed as the mean ± SEM.

1. Salamonsen, L. A. Tissue injury and repair in the female human reproductive tract. *Reproduction* **125**, 301–311 (2003).
2. Hawkins, S. M. & Matzuk, M. M. The menstrual cycle: basic biology. *Ann N Y Acad Sci* **1135**, 10–18 (2008).
3. Cross, J. C., Werb, Z. & Fisher, S. J. Implantation and the placenta: key pieces of the development puzzle. *Science* **266**, 1508–1518 (1994).
4. Caligioni, C. S. Assessing reproductive status/stages in mice. *Curr Protoc Neurosci* **Appendix 4**, Appendix 4I (2009).
5. Hemler, M. E. Targeting of tetraspanin proteins--potential benefits and strategies. *Nat Rev Drug Discov* **7**, 747–758 (2008).
6. Miyake, M., Koyama, M., Seno, M. & Ikeyama, S. Identification of the motility-related protein (MRP-1), recognized by monoclonal antibody M31-15, which inhibits cell motility. *J Exp Med* **174**, 1347–1354 (1991).
7. Wynne, F. *et al.* Mouse pregnancy-specific glycoproteins: tissue-specific expression and evidence of association with maternal vasculature. *Reproduction* **131**, 721–732 (2006).
8. Denzer, K., Kleijmeer, M. J., Heijnen, H. F., Stoorvogel, W. & Geuze, H. J. Exosome: from internal vesicle of the multivesicular body to intercellular signaling device. *J Cell Sci* **113 Pt 19**, 3365–3374 (2000).

9. Wubbolts, R. *et al.* Proteomic and biochemical analyses of human B cell-derived exosomes. Potential implications for their function and multivesicular body formation. *J Biol Chem* **278**, 10963–10972 (2003).
10. Caby, M. P., Lankar, D., Vincendeau-Scherrer, C., Raposo, G. & Bonnerot, C. Exosomal-like vesicles are present in human blood plasma. *Int Immunol* **17**, 879–887 (2005).
11. Valadi, H. *et al.* Exosome-mediated transfer of mRNAs and microRNAs is a novel mechanism of genetic exchange between cells. *Nat Cell Biol* **9**, 654–659 (2007).
12. Thery, C. *et al.* Molecular characterization of dendritic cell-derived exosomes. Selective accumulation of the heat shock protein hsc73. *J Cell Biol* **147**, 599–610 (1999).
13. Miyado, K. *et al.* Requirement of CD9 on the egg plasma membrane for fertilization. *Science* **287**, 321–324 (2000).
14. Le Naour, F., Rubinstein, E., Jasmin, C., Prenant, M. & Boucheix, C. Severely reduced female fertility in CD9-deficient mice. *Science* **287**, 319–321 (2000).
15. Kaji, K. *et al.* The gamete fusion process is defective in eggs of Cd9-deficient mice. *Nat Genet* **24**, 279–282 (2000).
16. Miyado, K. *et al.* The fusing ability of sperm is bestowed by CD9-containing vesicles released from eggs in mice. *Proc Natl Acad Sci U S A* **105**, 12921–12926 (2008).
17. Devaux, P. F. Protein involvement in transmembrane lipid asymmetry. *Annu Rev Biophys Biomol Struct* **21**, 417–439 (1992).
18. Park, K. R. *et al.* CD9 is expressed on human endometrial epithelial cells in association with integrins alpha(6), alpha(3) and beta(1). *Mol Hum Reprod* **6**, 252–257 (2000).
19. Hasuwa, H. *et al.* CD9 amino acids critical for upregulation of diphtheria toxin binding. *Biochem Biophys Res Commun* **289**, 782–790 (2001).
20. Dominguez, F. *et al.* Human endometrial CD98 is essential for blastocyst adhesion. *PLoS One* **5**, e13380 (2010).
21. Singh, H. & Aplin, J. D. Adhesion molecules in endometrial epithelium: tissue integrity and embryo implantation. *J Anat* **215**, 3–13 (2009).
22. Feral, C. C. *et al.* CD98hc (SLC3A2) participates in fibronectin matrix assembly by mediating integrin signaling. *J Cell Biol* **178**, 701–711 (2007).
23. Spits, H. & Di Santo, J. P. The expanding family of innate lymphoid cells: regulators and effectors of immunity and tissue remodeling. *Nat Immunol* **12**, 21–27 (2011).
24. Dimitriadis, E., White, C. A., Jones, R. L. & Salamonsen, L. A. Cytokines, chemokines and growth factors in endometrium related to implantation. *Hum Reprod Update* **11**, 613–630 (2005).
25. Rossi, M. *et al.* Identification of genes regulated by interleukin-1beta in human endometrial stromal cells. *Reproduction* **130**, 721–729 (2005).
26. Makkar, G., Ng, E. H., Yeung, W. S. & Ho, P. C. Excessive ovarian response is associated with increased expression of interleukin-2 in the periimplantation endometrium. *Fertil Steril* **91**, 1145–1151 (2009).
27. Fishman, P. *et al.* Prevention of fetal loss in experimental antiphospholipid syndrome by in vivo administration of recombinant interleukin-3. *J Clin Invest* **91**, 1834–1837 (1993).
28. Katano, K. *et al.* Low serum M-CSF levels are associated with unexplained recurrent abortion. *Am J Reprod Immunol* **38**, 1–5 (1997).
29. Ashkar, A. A., Di Santo, J. P. & Croy, B. A. Interferon gamma contributes to initiation of uterine vascular modification, decidual integrity, and uterine natural killer cell maturation during normal murine pregnancy. *J Exp Med* **192**, 259–270 (2000).
30. Stordeur, P. & Goldman, M. Interleukin-10 as a regulatory cytokine induced by cellular stress: molecular aspects. *Int Rev Immunol* **16**, 501–522 (1998).
31. Seder, R. A., Gazzinelli, R., Sher, A. & Paul, W. E. Interleukin 12 acts directly on CD4+ T cells to enhance priming for interferon gamma production and diminishes interleukin 4 inhibition of such priming. *Proc Natl Acad Sci U S A* **90**, 10188–10192 (1993).
32. Kaitu'u-Lino, T. J., Morison, N. B. & Salamonsen, L. A. Neutrophil depletion retards endometrial repair in a mouse model. *Cell Tissue Res* **328**, 197–206 (2007).
33. Semerad, C. L., Liu, F., Gregory, A. D., Stumpf, K. & Link, D. C. G-CSF is an essential regulator of neutrophil trafficking from the bone marrow to the blood. *Immunity* **17**, 413–423 (2002).
34. Chou, R. C. *et al.* Lipid-cytokine-chemokine cascade drives neutrophil recruitment in a murine model of inflammatory arthritis. *Immunity* **33**, 266–278 (2010).
35. Moser, B., Wolf, M., Walz, A. & Loetscher, P. Chemokines: multiple levels of leukocyte migration control. *Trends Immunol* **25**, 75–84 (2004).
36. Ferrara, N., Gerber, H. P. & LeCouter, J. The biology of VEGF and its receptors. *Nat Med* **9**, 669–676 (2003).
37. Kim, M. *et al.* VEGF-A regulated by progesterone governs uterine angiogenesis and vascular remodelling during pregnancy. *EMBO Mol Med* (2013).
38. Boesen, T. P., Soni, B., Schwartz, T. W. & Halkier, T. Single-chain vascular endothelial growth factor variant with antagonist activity. *J Biol Chem* **277**, 40335–40341 (2002).
39. Nothnick, W. B., Soloway, P. & Curry, T. E., Jr. Assessment of the role of tissue inhibitor of metalloproteinase-1 (TIMP-1) during the periovulatory period in female mice lacking a functional TIMP-1 gene. *Biol Reprod* **56**, 1181–1188 (1997).
40. Marzesco, A. M. *et al.* Release of extracellular membrane vesicles from microvilli of epithelial cells is enhanced by depleting membrane cholesterol. *FEBS Lett* **583**, 897–902 (2009).
41. Fan, X. *et al.* VEGF blockade inhibits angiogenesis and reepithelialization of endometrium. *FASEB J* **22**, 3571–3580 (2008).
42. Ng, Y. H. *et al.* Endometrial exosomes/microvesicles in the uterine microenvironment: a new paradigm for embryo-endometrial cross talk at implantation. *PLoS One* **8**, e58502 (2013).
43. Komada, Y. *et al.* Shedding of CD9 antigen into cerebrospinal fluid by acute lymphoblastic leukemia cells. *Blood* **76**, 112–116 (1990).
44. Epple, L. M. *et al.* Medulloblastoma exosome proteomics yield functional roles for extracellular vesicles. *PLoS One* **7**, e42064 (2012).
45. Blackman, M. R. *et al.* Human placental and pituitary glycoprotein hormones and their subunits as tumor markers: a quantitative assessment. *J Natl Cancer Inst* **65**, 81–93 (1980).
46. Baker, R. M., Hirschberg, C. B., O'Brien, W. A., Awerbuch, T. E. & Watson, D. Isolation of somatic cell glycoprotein mutants. *Methods Enzymol* **83**, 444–458 (1982).
47. Teranishi, A., Kuwata, A., Fumino, T., Hamai, H. & Shigeta, M. A theoretical model for single blastocyst transfer. *J Assist Reprod Genet* **26**, 327–334 (2009).
48. Paria, B. C., Huet-Hudson, Y. M. & Dey, S. K. Blastocyst's state of activity determines the "window" of implantation in the receptive mouse uterus. *Proc Natl Acad Sci U S A* **90**, 10159–10162 (1993).
49. Tamm, I. & Horsfall, F. L., Jr. Characterization and separation of an inhibitor of viral hemagglutination present in urine. *Proc Soc Exp Biol Med* **74**, 106–108 (1950).
50. Rankin, T. L. *et al.* Human ZP3 restores fertility in Zp3 null mice without affecting order-specific sperm binding. *Development* **125**, 2415–2424 (1998).
51. Fernandez-Shaw, S., Shorter, S. C., Naish, C. E., Barlow, D. H. & Starkey, P. M. Isolation and purification of human endometrial stromal and glandular cells using immunomagnetic microspheres. *Hum Reprod* **7**, 156–161 (1992).
52. Toshimori, K., Saxena, D. K., Tanii, I. & Yoshinaga, K. An MN9 antigenic molecule, equatorin, is required for successful sperm-oocyte fusion in mice. *Biol Reprod* **59**, 22–29 (1998).

Acknowledgments

This study was supported by a grant from The Ministry of Health, Labour and Welfare, and a Grant-in-aid for Scientific Research from The Ministry of Education, Culture, Sports, and Technology of Japan.

Author contributions

K.M. and T.H. conceived and designed the experiments. N.K., N.Y. and S.K. performed the experiments. K.M., T.H., N.K., H.S., M.M., N.I., Y.O. and A.U. analyzed the data. K.M., T.H. and N.K. wrote the manuscript and prepared figures. All authors reviewed the manuscript.

Additional information

Supplementary information accompanies this paper at http://www.nature.com/scientificreports

Competing financial interests: The authors declare no competing financial interests.

How to cite this article: Kawano, N. *et al.* Absence of CD9 reduces endometrial VEGF secretion and impairs uterine repair after parturition. *Sci. Rep.* **4**, 4701; DOI:10.1038/srep04701 (2014).

SCIENTIFIC REPORTS

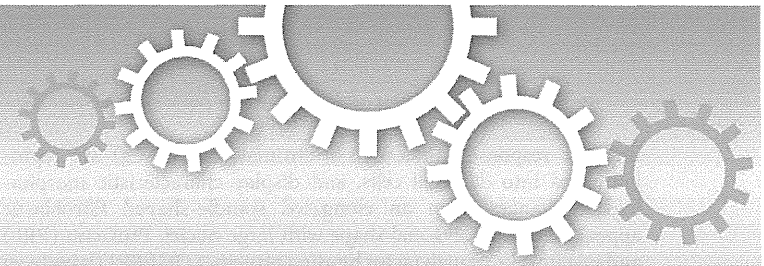

OPEN

SUBJECT AREAS:
STEM-CELL DIFFERENTIATION
MESENCHYMAL STEM CELLS

Received
6 January 2014

Accepted
10 March 2014

Published
8 April 2014

Correspondence and requests for materials should be addressed to T.H. (toshiohamatani@z3.keio.jp)

Derivation of human decidua-like cells from amnion and menstrual blood

Kana Sugawara[1,2], Toshio Hamatani[1], Mitsutoshi Yamada[1], Seiji Ogawa[1], Shintaro Kamijo[1], Naoaki Kuji[1], Hidenori Akutsu[2], Kenji Miyado[2], Yasunori Yoshimura[1] & Akihiro Umezawa[2]

[1]Department of Obstetrics and Gynecology, Keio University School of Medicine, 35 Shinanomachi Shinjuku-ku, Tokyo 160-8582, Japan, [2]Department of Reproductive Biology, National Research Institute for Child Health and Development, 2-10-1 Ohkura Setagaya-ku, Tokyo 157-8535, Japan.

We induced differentiation of human amnion-derived mesenchymal stem cells (AMCs) and menstrual blood-derived mesenchymal stem cells (MMCs) into endometrial stroma-like cells, which could be useful for cell therapy to support embryo implantation. Interestingly, the expression patterns of surface markers were similar among AMCs, MMCs, and endometrial stromal cells. In addition, whereas treatment with estrogen and progesterone was not very effective for decidualizing AMCs and MMCs, treatment with 8-Br-cAMP prompted remarkable morphological changes in these cells as well as increased expression of decidualization markers (prolactin and insulin-like growth factor binding protein-1) and attenuated expression of surface markers unique to mesenchymal stem cells. These results demonstrated that bone marrow-derived stem cells, which are considered a potential source of endometrial progenitor cells, as well as AMCs and MMCs show *in vitro* decidualization potential, which is characteristic of endometrial stromal cells.

Many infertile couples have achieved pregnancy by assisted reproductive technology (ART). However, despite having good-quality embryos for transfer, there are still women who experience repeated implantation failure even after several ART attempts[1,2]. Uterine receptivity is considered as another important factor for successful implantation and many studies have attempted to identify clinically useful markers of a receptive uterine state. However, such molecular markers related to repeated implantation failure have proven difficult to find, largely because uterine receptivity is regulated via the expression of various mediators, including cell adhesion molecules (e.g. cadherins and integrins), chemical mediators (e.g. prostaglandins), and cytokines (e.g. leukemia inhibitory factor and epithelial growth factor).

Thinning of endometrium has also been correlated with implantation failure, with causes including aging[3], and repeated invasive procedures such as dilation and curettage for miscarriage or early-stage endometrial cancer. Some studies have reported clinical benefits from ascorbic acid (vitamin C), tocopherol (vitamin E), pentoxifylline (PTX), or sildenafil for repeated implantation failure in patients with thin endometrium, although the effectiveness and molecular mechanisms by which such agent could improve the implantation process is not well established[4–6].

In studies to improve implantation rates, Landgren et al.[7] developed a coculture model of embryos with endometrial cells harvested from an endometrial biopsy taken at 4, 5, and 6 days after the lutenizing hormone (LH) peak in healthy women with normal menstrual cycles. The rate of pregnancy increased for embryos transferred after the coculture of embryo with endometrium than for embryos transferred after repeat ART[8]. However it is difficult to retrieve and culture endometrial cells from women whose endometrium has already become thin. Therefore we focused on mesenchymal stem cells (MSCs) as a source for this type of cell therapy using endometrial stroma-like cells. MSCs might also support embryo implantation by excreting cytokines and chemical mediators for adhesion, migration, or immunomodulation[9–11]. Indeed, fertility was restored in a patient with severe Asherman's syndrome treated using autologous bone marrow-derived MSC populations[12].

MSCs are multipotent, adherent stem cells capable of differentiating into osteoblasts, adipocytes, and chondroblasts[13], as well as endodermal lineages such as pancreatic islands[14,15] or hepatocytes[16,17], and ectodermal lineage such as neurons[14,18]. An earlier study verified that human bone marrow-derived MSC (BMCs) are potential progenitors of endometrial stromal cells by demonstrating their ability to decidualize[19]. Decidualization is a remodeling process designed to prepare endometrium for pregnancy that is induced by progesterone secreted from the ovaries in the luteal phase. This remodeling is necessary in a successful pregnancy to regulate trophoblast invasion, resist oxidative stress, and protect the placental semi-allograft against maternal

immune responses. Endometrial stromal cells (ESCs) are reprogrammed into decidual cells, and display characteristic morphological changes from an elongated spindle-shaped fibroblastic appearance to a polygonal shape with large nuclei. Prolactin (PRL) and insulin-like growth factor binding protein-1 (IGFBP1) have been widely used as phenotypic markers of decidual cells. In the current study, we hypothesized that if MSCs could differentiate into ESC-like cells, their treatment with agents known to promote decidualization could induce the expression of PRL and IGFBP1 in the MSC-derived cells. Indeed, AMCs and MMCs successfully differentiate into endometrial stroma-like cells presenting decidualization potential to the same extent as bone marrow-derived cells[19]. In this context, human amnion in particular could be a powerful therapeutic cell source because not only is it an easily accessible tissue for cell harvesting, it does not require co-administration of immunosuppressive agent or matching of MHC typing for immunological tolerance.

Results

Characterization of human endometrial cells. Immunofluorescence staining and flow cytometric analysis of cultured human endometrial cells and MRC5 fibroblasts revealed both to be positive for vimentin and negative for cytokeratin, whereas a human carcinoma cell line, HeLa cells, was positive for both vimentin and cytokeratin. (Fig. 1A–E). By flow cytometry, the endometrial cells and fibroblasts were negative for CD9 and positive for CD10, whereas HeLa cells were positive for CD9 and negative for CD10. Together, these results confirmed that the endometrial cells were stromal in origin, compared to the epithelial-derived HeLa cells.

We then investigated cell surface marker expressions of ESCs, AMCs, MMCs, BMCs, and MRC5 by flow cytometric analysis on the initial day of treatment (day 0) (Fig. 1F). Although there is no marker specific to MSCs, they are known to express CD73, CD90, and CD105[20], and the AMCs and MMCs tested herein indeed expressed these cell surface markers as well as CD54, CD166 and HLA-ABC, but not HLA-DR (Supplementary Fig. S1). This result confirmed the earlier studies of our group demonstrating that both AMCs and MMCs express MSC markers such as CD29, CD44, CD59, CD73, CD105, and CD166, but not hematopoietic markers such as CD14, CD34, and CD45[21–23]. None of the cells analyzed in the present study expressed hematopoietic lineage markers such as CD34 or monocyte-macrophage antigens such as CD14 (a marker for macrophage and dendritic cells) and CD45 (leukocyte common antigen), suggesting no contaminating hematopoietic cells. Lastly, and interestingly, the surface marker expression patterns of AMCs and MMCs were very similar to those of ESCs.

Decidual differentiation by treatment with $E_2 + P_4$. Human ESCs showed distinct morphological changes following treatment with $E_2 + P_4$, from spindle-shaped to large round cells with large round nuclei, whereas AMCs, MMCs, and BMCs showed no remarkable morphological changes (Fig. 2A). Flow cytometric analysis of ESCs, AMCs, MMCs, BMCs, and MRC5 fibroblasts on day 14 of treatment with $E_2 + P_4$ (Fig. 2B and Supplementary Fig. S2) also showed no remarkable changes in surface marker expressions compared to those on day 0.

Immunofluorescence staining was also performed to assess the expression of decidualization markers (PRL and IGFBP1) at day 0, 7, and 14 after treatment with $E_2 + P_4$ (Fig. 3). None of these markers were expressed at day 0 in ESCs, AMCs, MMCs, and BMCs, but PRL and IGFBP1 were expressed in ESCs on days 7 and 14 following treatment with $E_2 + P_4$ (Figs. 3A and 3B). AMCs also showed clear expression of PRL on days 7 and 14 following treatment, but only faint IGFBP1 expression (Figs. 3C and 3D), while the reverse pattern was observed in MMCs (Figs. 3E and 3F). Finally, both PRL and IGFBP1 were faintly expressed in BMCs (Figs. 3G and 3H).

The qRT-PCR analysis of expression changes in *PRL* and *IGFBP1* mRNAs with $E_2 + P_4$ treatment (Figs. 2C and 2D) revealed upregulation of *PRL* in each cell type on days 7 and 14 following treatment compared to day 0 levels, whereas *IGFBP1* was upregulated only in ESCs on days 7 and 14 compared to day 0, and not in AMCs, MMCs, and BMCs.

Decidual differentiation by treatment with cAMP. The human ESCs, AMCs, MMCs, and BMCs all showed morphological changes from a spindle-shaped appearance to large rounded cells with large round nuclei following treatment with cAMP (Fig. 4A). In addition, flow cytometry revealed that CD90, CD105, and CD166 were attenuated in the AMCs and ESCs on day 14 of the cAMP treatment (Fig. 4B and Supplementary Fig. S3) compared to day 0 levels. Together, these changes suggested that cAMP upregulates decidual differentiation in AMCs. On the other hand, CD105 and CD166 in MMCs as well as CD90 and CD166 in BMCs were unchanged, suggesting that AMCs could have more potential for differentiation to ESCs than MMCs and BMCs.

Immunofluorescence staining showed no expression of decidualization markers (PRL and IGFBP1) at day 0 in the four cell types, but positive staining for PRL on days 7 and 14 of the cAMP treatment (Fig. 5A, 5C, 5E and 5G). Although IGFBP1 was also expressed in all the types of cells on day 7 and day 14, AMCs and MMCs showed more remarkable IGFBP1 expression on day 7 compared to day 14.

Finally, the qRT-PCR analysis showed that *PRL* transcripts were more abundant in all the cell types on days 7 and 14 following cAMP treatment than on day 0 (Figs. 4C and 4D), whereas *IGFBP1* was upregulated in AMCs and ESCs, but not in MMCs and BMCs. These results suggested that AMCs treated with cAMP have the closest decidualization potential to ESCs.

Discussion

Insufficient response of MSCs to $E_2 + P_4$. In this study, we investigated whether human MSCs such as AMCs and MMCs could be differentiated *in vitro* into endometrial stroma-like cells using decidualization stimuli and analysis of cellular morphology and expression of decidualization markers (PRL and IGFBP1). The MSCs and ESCs were treated with $E_2 + P_4$ to mimic the normal endocrinological condition in the secretory phase of a human menstrual cycle. ESCs and BMCs were considered as positive controls. Unexpectedly, not only the AMCs and MMCs, but also the BMCs, failed to show remarkable decidual changes with $E_2 + P_4$ treatment. Sustained expression of cell surface markers, no marked morphological changes, and little expression of IGFBP1 in MSCs treated with $E_2 + P_4$ indicated that these cells are not sufficiently responsive to such stimulation to induce differentiation, supporting previous results by Aghajanova. et al.[19] in BMCs treated with $E_2 + P_4$. The qRT-PCR in this study showed significant expression of progesterone receptors (PR) and estrogen receptors (ESR1 and ESR2) in AMCs, MMCs, and ESCs (Supplementary Fig. S5). Aghajanova et al. also demonstrated *PR*, *ESR1*, and *ESR2* mRNA expression in BMCs and ESCs, but this expression was not significantly influenced by cAMP treatment of the cells[19]. Furthermore, with respect to secretory-phase endometrium *in vivo*, decidualization of the superficial endometrial layers is only apparent ~10 days after the postovulatory increase in progesterone levels. All these observations indicate that additional signals other than the progesterone signaling are required to initiate decidualization. Interestingly, trichostatin A (TSA), a specific histone deacetylase (HDACs) inhibitor, enhanced the upregulation of PRL and IGFBP1 in a dose-dependent manner in cultured endometrial stromal cells following treatment with $E_2 + P_4$[24]. In addition, IGFBP1 expression induced by cAMP was associated with the histone acetylation status of the promoter region in human endometrial stromal cells[25]. Based on these results, we speculated that TSA might be effective in enhancing IGFBP1 expression in AMCs and MMCs treated with $E_2 + P_4$; however, AMCs and MMCs treated with $E_2 + P_4$ and several concentrations

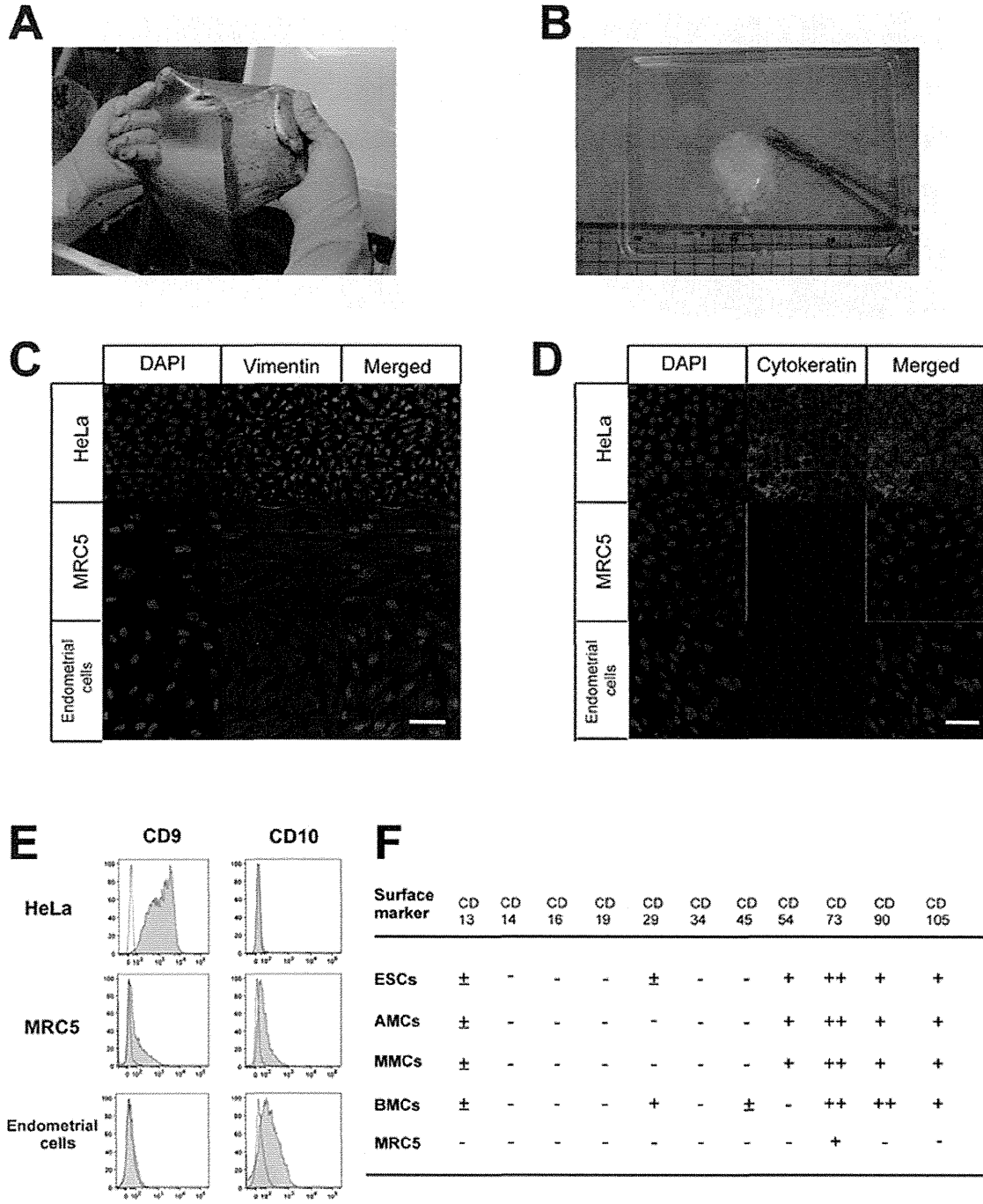

F

Surface marker	CD 13	CD 14	CD 16	CD 19	CD 29	CD 34	CD 45	CD 54	CD 73	CD 90	CD 105	CD 166	HLA -DR
ESCs	±	-	-	-	±	-	-	+	++	+	+	+	-
AMCs	±	-	-	-	-	-	-	+	++	+	+	+	-
MMCs	±	-	-	-	-	-	-	+	++	+	+	+	-
BMCs	±	-	-	-	+	-	±	-	++	++	+	+	-
MRC5	-	-	-	-	-	-	-	-	+	-	-	-	-

Figure 1 | Characterization of endometrial cells, amnion-derived cells, and menstrual blood-derived cells. (A), Macroscopic view of human amniotic membrane. (B), The amniotic membrane was cut into pieces of approximately 2 mm^3 in size. (C and D), Laser confocal microscopic view of immunofluorescence staining of endometrial cells, HeLa cells, and MRC5 fibroblasts in culture with anti-vimentin (red) (C) and anti-cytokeratin antibodies (green) (D), DAPI staining (blue). Scale bars, 100 μm. (E), Surface marker (CD9 or CD10) expression of endometrial cells, HeLa cells, and MRC5 fibroblasts. White and grey areas indicate reactivity of antibodies for isotype controls and that for CD9 or CD10, respectively. (F), Summary of flow cytometric analysis of endometrial stromal cells (ESCs), amnion-derived mesenchymal stem cells (AMCs), menstrual blood-derived mesenchymal stem cells (MMCs), bone marrow-derived mesenchymal stem cells (BMCs), and MRC5 fibroblasts before treatment. The shift in peak histogram value of flow cytometric data was measured and classified into four groups: −, from negative to 2 log shift; ±, 2 log shift from negative control; +, 3 log shift from negative control; ++, 4 log shift from negative control.

of TSA showed no enhancement of IGFBP1 expression (Supplemental Fig. S4). We therefore further investigated the decidualization potential of MSCs in the current study using cAMP, a well-known and common facilitator of decidualization[19,25].

Attenuation of cell surface markers for MSCs during successful decidualization by cAMP. Estrogen and progesterone bind to nuclear receptor proteins for nuclear importing, where they bind DNA directly to regulate transcription, whereas cAMP activates the protein

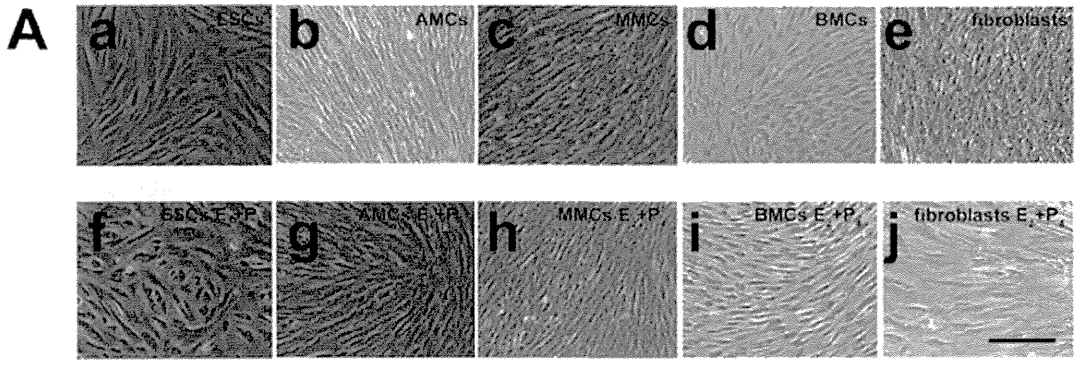

B

Surface marker	CD 13	CD 14	CD 16	CD 19	CD 29	CD 34	CD 45	CD 54	CD 73	CD 90	CD 105	CD 166	HLA -DR
ESCs	±	-	-	-	+	-	-	+	+	+	+	+	-
AMCs	±	-	-	-	+	-	-	+	++	+	+	+	-
MMCs	+	-	-	-	+	-	-	+	++	+	+	+	-
BMCs	±	-	-	-	±	-	±	+	++	++	+	+	-
MRC5	-	-	-	-	-	-	-	-	-	-	+	-	-

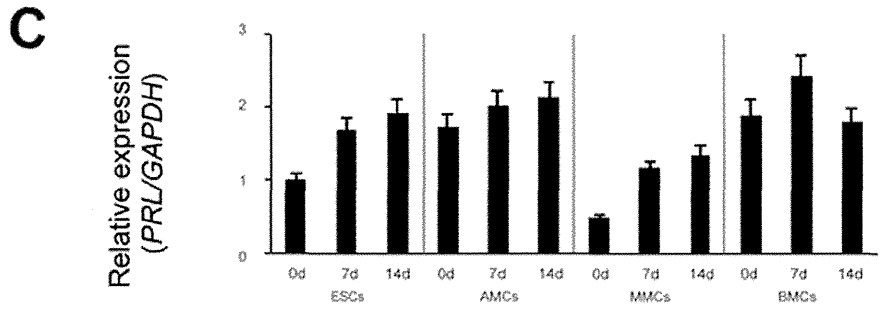

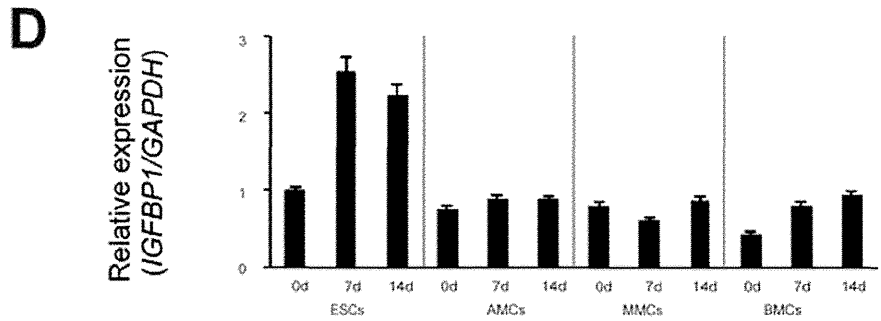

Figure 2 | Morphological changes and alteration of flow cytometric profiles in mesenchymal stem cells treated with E_2 + P_4. (A), Morphological changes in endometrial stromal cells (ESCs) (a, f), amnion-derived mesenchymal stem cells (AMCs) (b, g), menstrual blood-derived mesenchymal stem cells (MMCs) (c, h), bone marrow-derived mesenchymal stem cells (BMCs) (d, i), and MRC5 fibroblasts (e, j) before (a–c) and after (f–j) treatment with 10 nM E_2 and 1 μM P_4 (E_2 + P_4) for 14 days. Scale bars, 200 μm. (B), Summary of flow cytometric analysis of ESCs, AMCs, MMCs, BMCs, and MRC5 fibroblasts treated with E_2 + P_4 for 14 days. We measured the shift of peak histogram value for the flow cytometric data and defined each result by the aforementioned criteria. (C), PRL mRNA expression in ESCs, AMCs, MMCs, and BMCs treated with E_2 + P_4 for 0, 7, and 14 days. (D), IGFBP1 mRNA expression in ESCs, AMCs, MMCs, and BMCs treated with E_2 + P_4 for 14 days.

kinase A (PKA) pathway and a catalytic subunit of PKA translocates into the cell nucleus to phosphorylate cAMP response element-binding protein (CREB). Activated CREB then enhances gene transcription via cAMP response element (CRE)[26]. In this study, cAMP treatment of AMCs and MMCs produced morphological changes characteristic of decidual cells, and PRL and IGFBP1 expression increases consistent with those seen in ESCs. AMCs and MMCs were thus demonstrated to have decidualization potential.

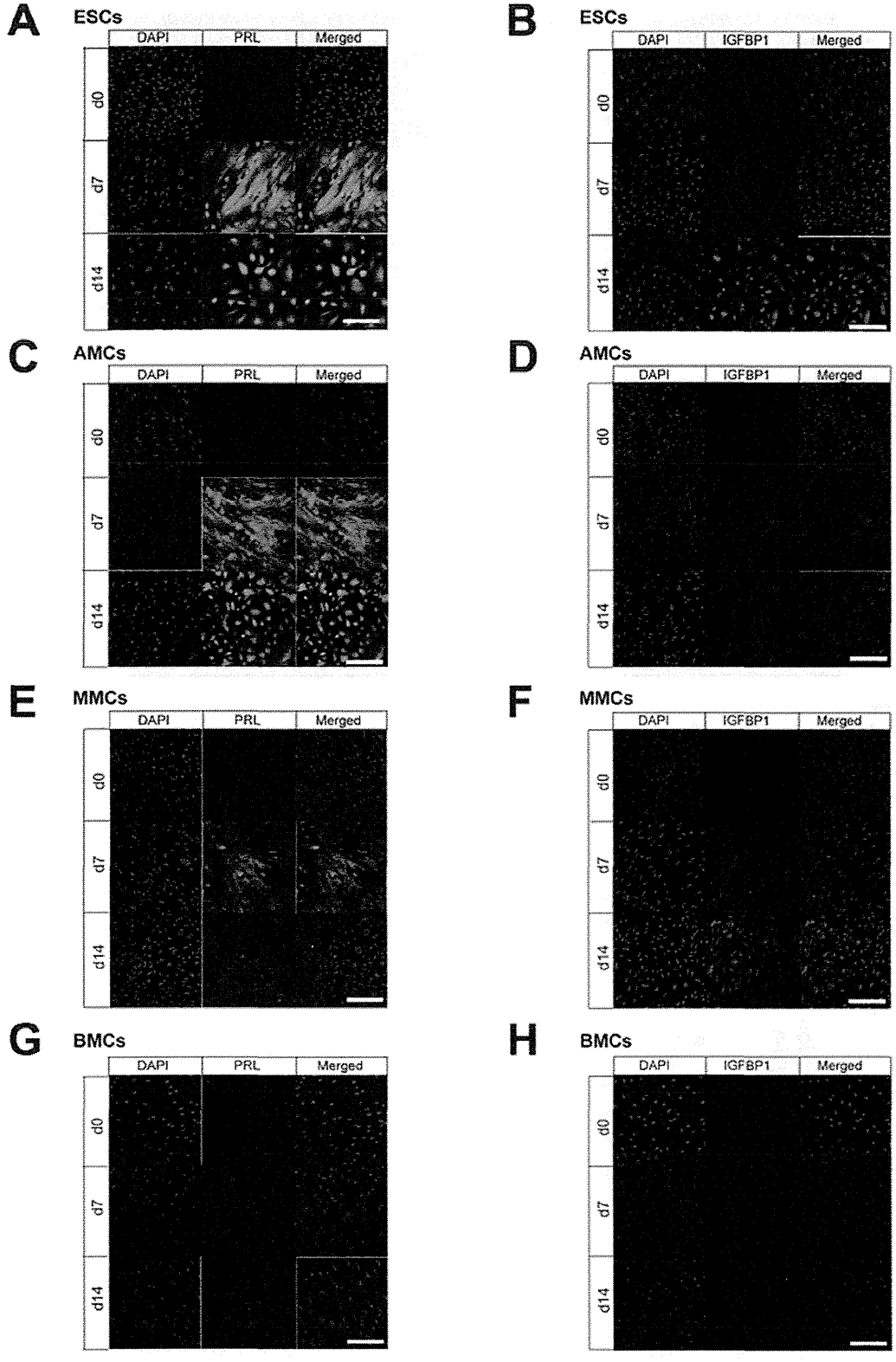

Figure 3 | Immunofluorescence staining of decidualization markers (PRL and IGFBP1) in mesenchymal stem cells treated with $E_2 + P_4$. Laser confocal microscopy of PRL immunofluorescence staining (green signals in A, C, E, and G) and IGFBP1 (red signals in B, D, F, H) in endometrial stromal cells (ESCs) (A and B), amnion-derived mesenchymal stem cells (AMCs) (C and D), menstrual blood-derived mesenchymal stem cells (MMCs) (E and F), and bone marrow-derived mesenchymal stem cells BMCs (G and H) treated with $E_2 + P_4$ for 0, 7, or 14 days. Scale bars, 200 μm.

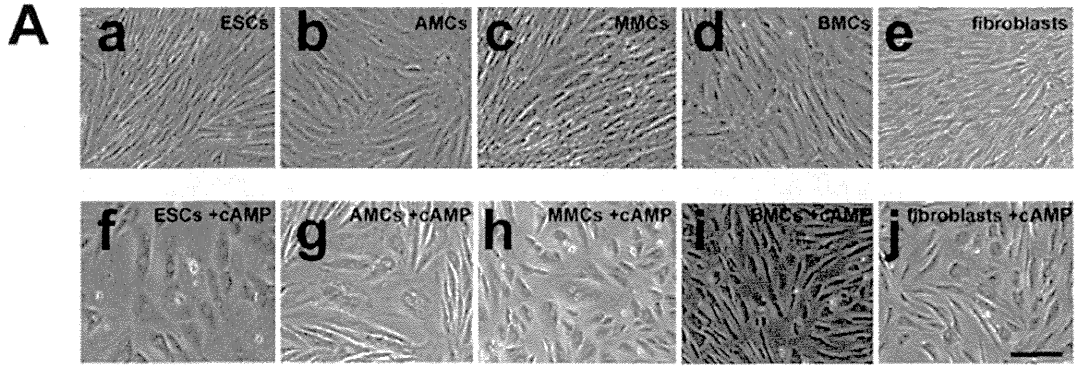

B

Surface marker	CD 13	CD 14	CD 16	CD 19	CD 29	CD 34	CD 45	CD 54	CD 73	CD 90	CD 105	CD 166	HLA -DR
ESCs	-	-	-	-	-	-	-	+	++	-	±	±	-
AMCs	±	-	-	-	-	-	-	±	++	±	±	±	-
MMCs	+	±	±	±	±	±	±	++	++	±	+	+	±
BMCs	±	±	-	-	±	-	-	+	+	++	±	+	-
MRC5	-	-	-	-	-	-	-	-	-	-	-	-	-

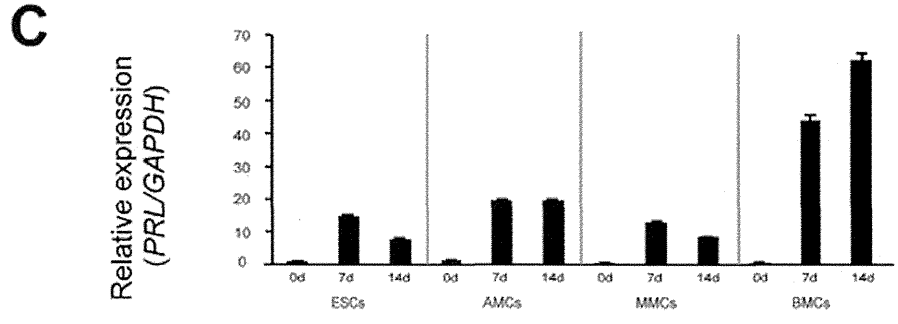

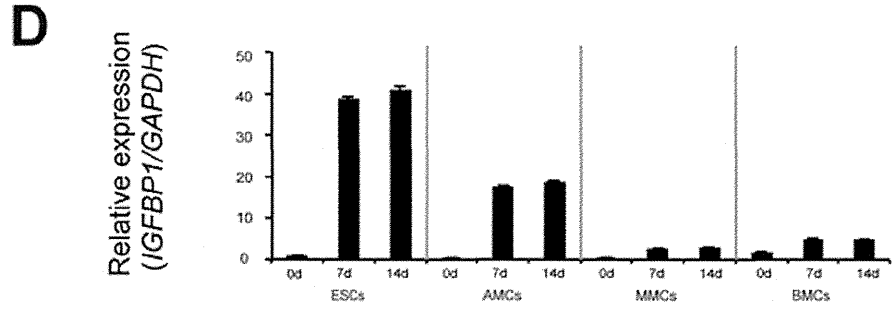

Figure 4 | Morphological changes and alteration of flow cytometric profiles in mesenchymal stem cells treated with cAMP. (A), Morphological changes of endometrial stromal cells (ESCs) (a, f), amnion-derived mesenchymal stem cells (AMCs) (b, g), menstrual blood-derived mesenchymal stem cells (MMCs) (c, h), bone marrow-derived mesenchymal stem cells (BMCs) (d, i), and MRC5 fibroblasts (e, j) before (a–e) and (f–j) after treatment with 1 mM 8-Br-cAMP for 14 days. Scale bars, 200 μm. (B), Summary of flow cytometric analysis of ESCs, AMCs, MMCs, BMCs, and MRC5 fibroblasts treated with 1 mM 8-Br-cAMP for 14 days. We measured the shift of peak histogram value for the flow cytometric data and defined each result by the aforementioned criteria. (C), PRL mRNA expression in ESCs, AMCs, MMCs, and BMCs treated with 1 mM 8-Br-cAMP for 0, 7, and 14 days. (D), IGFBP1 mRNA expression in ESCs, AMCs, MMCs, and BMCs treated with 1 mM 8-Br-cAMP for 0, 7, and 14 days.

In the cell surface marker analysis, the attenuation of CD90, CD105, and CD166 during decidualization was notable. Such a response by these well-defined human MSCs markers could indicate the direction of differentiation in MSCs treated with cAMP. Furthermore, CD90 is known to regulate adhesion to T cells in MSCs, and a decrease in CD90-positive cells might be a novel predictive marker of immunosuppressive activity[27]. Based on these observations, the decreased rate of CD90-positive cells with cAMP

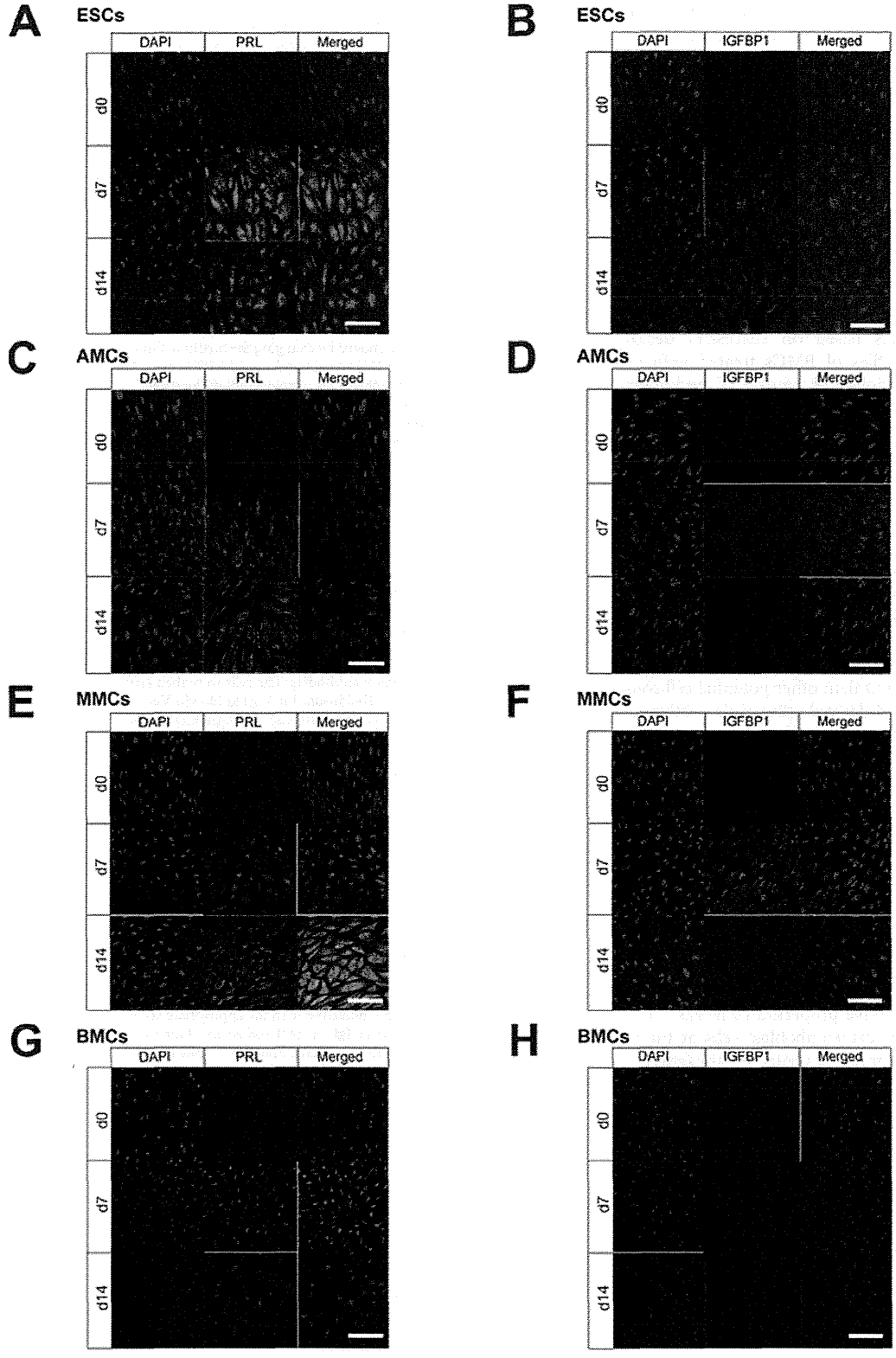

Figure 5 | Immunofluorescence staining of decidualization markers (PRL and IGFBP1) in mesenchymal stem cells treated with cAMP. Laser confocal microscopic view of immunofluorescence staining for PRL (green signals in A, C, E, and G) and IGFBP1 (red signals in B, D, F, and H) in endometrial stromal cells (ESCs) (A and B), amnion-derived mesenchymal stem cells (AMCs) (C and D), menstrual blood-derived mesenchymal stem cells (MMCs) (E and F), bone marrow-derived mesenchymal stem cells (BMCs) (G and H) treated with 1 mM 8-Br-cAMP for 0, 7, and 14 days. Scale bars, 200 μm.

observed in the current study may indicate immunosuppression in AMCs and MMCs that is advantageous in terms of their potential clinical application. CD105 (endoglin) is a reliable marker for highly multipotent human MSCs, with CD105-expressing MSCs showing high efficiency in repairing the infarcted heart[28]. Therefore, the disappearance of CD105 with cAMP treatment would ensure differentiation of MSCs[29,30]. Collectively, our findings indicated that administration of cAMP effectively leads to differentiation and decidualization of AMCs and MMCs.

Advantages of AMCs and MMCs. It has been reported that endometrial stem cells are CD45-positive cells around blood vessels and likely to be derived from BMCs[31]. A previous study also indicated that BMCs might be a source of endometrial stem/progenitor cells based on successful decidualization and gene expression profiles of BMCs treated with cAMP[19]. If BMCs are indeed a physiological source of endometrial progenitor cells, BMCs could be ideal for use in cell-based therapies for infertile women who have thinning of the endometrium. However, our findings revealed that not only BMCs, but AMCs and MMCs, also showed decidualization potential, and that all three cell types showed a similar profile of cell surface marker expression to that of ESCs. Therefore, the current study suggested that BMCs is not the only such candidate for cell therapy.

In general, the collection of bone marrow is an invasive technique performed with a biopsy needle that requires local or even general anesthesia, and occasionally raises an ethical problem. On the other hand, human amnion is non-invasively and adequately obtained at delivery. Therefore, human amnion is more simply accessed with informed consent than other potential cell sources. Human primary menstrual blood-derived cells are also obtained by a simple, safe, and painless procedure, and efficiently expanded in vitro. In particular, the MMC-derived cells can be used for autologous transplantation. Accordingly, if culture condition for MMCs could be more successfully optimized for differentiation to ESCs, MMCs would be definitely useful for eventual cell-based therapies for infertility.

Furthermore, previous studies suggested that human amnion has the potential for immunological tolerance[23,32]. AMCs are known to express less MHC compared to other MSCs, which is important in host tolerance. Cells that do not express MHC are potentially recognized by the immune system as non-self cells and accordingly, attacked by natural killer (NK) cells. A soluble factor such as the non-classic MHC class I antigen, HLA-G, is also critical for the immunosuppressive properties of MSCs[33]. HLA-G is expressed on the extravillous cytotrophoblast cells at the fetomaternal interface and plays a major role in protecting the fetus from maternal rejection by NK cells[34,35]. HLA-G thus blocks the immunological response of NK cells[36] and induces regulatory T cells[37], which is a requisite condition of immunological tolerance[35,38]. We previously showed by western blotting that HLA-G is also expressed in placenta-derived tissues including amnion[23]. Thus, AMC-derived cells have several advantages for application to cell-based therapy.

Based on the results of our current study, AMCs and MMCs in addition to BMCs show potential for decidualization, and are therefore candidate cell sources for therapy to support implantation and placentation. The current study provides novel and important information on AMCs and MMCs treated with cAMP as a model of decidualization.

Methods

Tissue isolation and cell culture. All experiments involving human cells and tissues were performed according to the Tenets of the Declaration of Helsinki and were approved by the Ethics Committee of the National Institute for Child and Health Development, Tokyo. Signed informed consent was obtained from all donors, and all specimens were irreversibly de-identified. Human endometrium was obtained from a patient undergoing hysterectomy due to myoma uteri and human placenta was collected after selective caesarean section delivery.

Human amnion-derived cells were isolated using the explant culture method, in which the cells were outgrown from pieces of amnion. Briefly, the amnion was cut into pieces of approximately 2 mm^3 in size, which were then washed in Dulbecco's modified Eagle's medium (DMEM) (high glucose; Sigma) supplemented with 100 U/ml penicillin-streptomycin (Gibco). Some pieces were attached to the substratum in a 10-cm dish. The cells migrated out from the cut ends after approximately 20 days of incubation at 37°C in 5% CO_2. The migrated cells were harvested with Dulbecco's phosphate-buffered saline containing 0.1% trypsin and 0.25 mM EDTA for 5 min at 37°C and counted. The harvested cells were then re-seeded at a density of 3×10^5 cells in 10-cm dishes. Once confluent, the cell monolayers were subcultured at a 1 : 8 split ratio onto new 10-cm dishes, and the culture medium was replaced with fresh DMEM supplemented with 10% fetal bovine serum (FBS) and 100 U/ml penicillin-streptomycin every 3 or 4 days[22].

Menstrual blood samples (n = 21) were collected in DMEM containing 100 U/ml penicillin-streptomycin and 2% FBS, and processed within 24 h. The centrifuged pellets containing endometrium-derived cells were resuspended in high-glucose DMEM with 10% FBS and penicillin-streptomycin, and then maintained at 37°C in a humidified atmosphere containing 5% CO_2 to attach for 48 h. Non-adherent cells were removed by changing the medium. Once sub-confluent, the cells were harvested with 0.25% trypsin and 1 mM EDTA, and plated to new dishes. After 2–3 passages, the attached cells were devoid of blood cells[21].

A human bone marrow-derived mesenchymal cell line, 3F0664 was purchased from Lonza (PT-2501, Basel, Switzerland) and cultured in the mesenchymal stem-cell-basal-medium (MSCBM)-Medium-BulletKit (PT-3238, Lonza). The normal human fetal fibroblast cell line MRC5 was also passaged in DMEM supplemented with 10% (v/v) FBS and 100 U/ml penicillin-streptomycin. Cultures were maintained at 37°C with 5% CO_2 in a humidified atmosphere.

For decidual differentiation, human endometrial cells, amnion-derived cells, menstrual blood-derived cells, bone marrow-derived cells, and MRC5 were first cultured as described above, then trypsinized and plated in 10-cm plates. Nearly confluent cells were cultured for 0, 7, and 14 days in low-serum medium (2% FBS) supplemented with: 1) 10 nM estrogen (E_2) and 1 μM progesterone (P_4) or 2) 1 mM 8-Br-cAMP (cAMP) (Sigma-Aldrich, Saint Louis, MO, USA).

Flow cytometric analysis. Cells were incubated for 20 min at 4°C with primary antibodies or isotype-matched control antibodies, followed by immunofluorescent secondary antibodies. The cells were then analyzed on a FACS Aria™ IIIu Cellsorter (Becton Dickinson, Inc.) using FlowJo Ver.7 (Tree Star, Inc.). Antibodies against human CD9, CD10, CD13, CD14, CD16, CD19, CD29, CD31, CD34, CD44, CD45, CD54, CD55, CD59, CD73, CD90, CD105, CD133, CD146, CD166, HLA-ABC, and HLA-DR were purchased from Beckman Coulter, Immunotech (Marseille, France), BD Pharmingen and BioLegend (San Diego, CA, USA)[21,22]. Supplementary table S1 shows the list of CD antigens investigated in this study[39–49].

Immunofluorescence staining. The immunofluorescence staining was performed as previously described[50]. Briefly, cells were fixed with 4% paraformaldehyde for 10 min at 4°C, treated with 0.1% Triton X-100 (Sigma) in PBS for 15 min at RT, and then incubated for 30 min at RT in protein-blocking solution consisting of PBS supplemented with 5% FBS. The samples were then incubated overnight with the following primary antibodies diluted in PBS: an anti-prolactin mouse monoclonal antibody, (QED Bioscience, San Diego, CA, USA), anti-IGFBP1 mouse monoclonal antibody (Santa Cruz Biotechnology, Dallas, Texas, CA, USA), anti-vimentin mouse monoclonal antibody, V9, (DAKO, Tokyo, Japan), and an anti-cytokeratin mouse monoclonal antibody, AE1 + AE3, (DAKO). Tissues were washed twice for 5 min in PBS and incubated with the appropriate secondary antibodies (Alexa Fluor 488 goat anti-mouse IgG, 1 : 600 and Alexa Fluor 546 goat anti-mouse IgG, 1 : 600; Life Technologies, Grand Island, NY). Nuclei were counterstained with 4′, 6-diamidino-2-phenylindole (DAPI; Biotium, CA, USA) for 30 min at RT followed by 10 final 5-min PBS washes before being cover slipped using mounting medium. Omission of primary antibodies served as a negative control.

Quantitative reverse transcriptase-polymerase chain reaction (qRT- PCR) analysis. Total cellular RNA was isolated from cells using an RNeasy Plus Mini Kit (Qiagen, Hilden, Germany) according to the manufacturer's protocol. Total RNA (2.5 μg each) for quantitative RT-PCR was converted to cDNA using an Oligo (dT) primer with Superscript VILO™ cDNA Synthesis Kit (Life Technologies Corp., Carlsbad, CA, USA), according to the manufacturer's manual. The cDNA template was amplified by thermal cycle reactions (Quant Studio™ 12 K Flex Real-Time PCR System) using the Platinum SYBR Green qPCR SuperMix-UDG (Life Technologies Corp.) under the following reaction conditions: 40 cycles of PCR (95°C for 15 s and 60°C for 1 min) after an initial denaturation (95°C for 2 min). Fluorescence was monitored during every PCR cycle at the annealing step. The authenticity and size of the PCR products were confirmed by a melting curve analysis using software provided by Applied Biosystems. mRNA levels were normalized using *GAPDH* as a housekeeping gene. Primers used to amplify a cDNA fragment for human PRL and IGFBP1 were the following: PRL, 5′-CATCAACAGCTGCCACACTT-3′ (F) and 5′-CGTTTGGTTTGCTCCTCAAT-3′ (R); IGFBP1, 5′-CTATGATGGCTCGAAGGCTC-3′ (F) and 5′-TTCTTGTTGCAGTTTGGCAG-3′ (R).

1. Lee, T. H. *et al.* Embryo quality is more important for younger women whereas age is more important for older women with regard to in vitro fertilization outcome and multiple pregnancy. *Fertil Steril* **86**, 64–69 (2006).

2. Navot, D. *et al.* Poor oocyte quality rather than implantation failure as a cause of age-related decline in female fertility. *Lancet* **337**, 1375–1377 (1991).
3. Amir, W. *et al.* Predicting factors for endometrial thickness during treatment with assisted reproductive technology. *Fertil Steril* **87**, 799–804 (2007).
4. Senturk, L. M. & Erel, C. T. Thin endometrium in assisted reproductive technology. *Curr Opin Obstet Gynecol* **20**, 221–228 (2008).
5. Sallam, H. N. Embryo transfer: factors involved in optimizing the success. *Curr Opin Obstet Gynecol* **17**, 289–298 (2005).
6. Check, J. H. *et al.* Neither sildenafil nor vaginal estradiol improves endometrial thickness in women with thin endometria after taking oral estradiol in graduating dosages. *Clin Exp Obstet Gynecol* **31**, 99–102 (2004).
7. Landgren, B. M., Johannisson, E., Stavreus-Evers, A., Hamberger, L. & Eriksson, H. A new method to study the process of implantation of a human blastocyst in vitro. *Fertil Steril* **65**, 1067–1070 (1996).
8. Eyheremendy, V. *et al.* Beneficial effect of autologous endometrial cell coculture in patients with repeated implantation failure. *Fertil Steril* **93**, 769–773 (2010).
9. Lee, E. J. *et al.* Spherical bullet formation via E-cadherin promotes therapeutic potency of mesenchymal stem cells derived from human umbilical cord blood for myocardial infarction. *Mol Ther* **20**, 1424–1433 (2012).
10. Qiu, Y., Marquez-Curtis, L. & Janowska-Wieczorek, A. Mesenchymal stromal cells derived from umbilical cord blood migrate in response to complement C1q. *Cytotherapy* **14**, 285–295 (2012).
11. Moorefield, E. C. *et al.* Cloned, CD117 selected human amniotic fluid stem cells are capable of modulating the immune response. *PLoS One* **6**, e26535 (2011).
12. Gargett, C. E. & Healy, D. L. Generating receptive endometrium in Asherman's syndrome. *J Hum Reprod Sci* **4**, 49–52 (2011).
13. Pittenger, M. F. *et al.* Multilineage Potential of Adult Human Mesenchymal Stem Cells. *Science* **284**, 143–147 (1999).
14. Miki, T., Lehmann, T., Cai, H., Stolz, D. B. & Strom, S. C. Stem cell characteristics of amniotic epithelial cells. *Stem Cells* **23**, 1549–1559 (2005).
15. Santos, T. M. *et al.* Expression of pancreatic endocrine markers by mesenchymal stem cells from human umbilical cord vein. *Transplant Proc* **42**, 563–565 (2010).
16. Lee, K. D. *et al.* In vitro hepatic differentiation of human mesenchymal stem cells. *Hepatology* **40**, 1275–1284 (2004).
17. Pournasr, B. *et al.* In vitro differentiation of human bone marrow mesenchymal stem cells into hepatocyte-like cells. *Arc Iran Med* **14**, 244–249 (2011).
18. Dezawa, M. *et al.* Specific induction of neuronal cells from bone marrow stromal cells and application for autologous transplantation. *J Clin Invest* **113**, 1701–1710 (2004).
19. Aghajanova, L., Horcajadas, J. A., Esteban, F. J. & Giudice, L. C. The bone marrow-derived human mesenchymal stem cell: potential progenitor of the endometrial stromal fibroblast. *Biol Reprod* **82**, 1076–1087 (2010).
20. Diaz-Prado, S. *et al.* Human amniotic membrane as an alternative source of stem cells for regenerative medicine. *Differentiation* **81**, 162–171 (2011).
21. Cui, C. H. *et al.* Menstrual blood-derived cells confer human dystrophin expression in the murine model of Duchenne muscular dystrophy via cell fusion and myogenic transdifferentiation. *Mol Biol Cell* **18**, 1586–1594 (2007).
22. Kawamichi, Y. *et al.* Cells of extraembryonic mesodermal origin confer human dystrophin in the mdx model of Duchenne muscular dystrophy. *J Cell Physiol* **223**, 695–702 (2010).
23. Tsuji, H. *et al.* Xenografted human amniotic membrane-derived mesenchymal stem cells are immunologically tolerated and transdifferentiated into cardiomyocytes. *Circ Res* **106**, 1613–1623 (2010).
24. Sakai, N. *et al.* Involvement of histone acetylation in ovarian steroid-induced decidualization of human endometrial stromal cells. *J Biol Chem* **278**, 16675–16682 (2003).
25. Tamura, I. *et al.* Induction of IGFBP-1 expression by cAMP is associated with histone acetylation status of the promoter region in human endometrial stromal cells. *Endocrinology* **153**, 5612–5621 (2012).
26. Malumbres, M. & Pellicer, A. RAS pathways to cell cycle control and cell transformation. *Front Biosci* **3**, d887–912 (1998).
27. Campioni, D. *et al.* A decreased positivity for CD90 on human mesenchymal stromal cells (MSCs) is associated with a loss of immunosuppressive activity by MSCs. *Cytometry B Clin Cytom* **76**, 225–230 (2009).
28. Gaebel, R. *et al.* Cell origin of human mesenchymal stem cells determines a different healing performance in cardiac regeneration. *PLoS One* **6**, e15652 (2011).
29. Rosu-Myles, M., Fair, J., Pearce, N. & Mehic, J. Non-multipotent stroma inhibit the proliferation and differentiation of mesenchymal stromal cells in vitro. *Cytotherapy* **12**, 818–830 (2010).
30. Jin, H. J. *et al.* Down-regulation of CD105 is associated with multi-lineage differentiation in human umbilical cord blood-derived mesenchymal stem cells. *Biochem Biophys Res Commun* **381**, 676–681 (2009).
31. Bratincsák, A. *et al.* CD45-positive blood cells give rise to uterine epithelial cells in mice. *Stem Cells* **25**, 2820–2826 (2007).
32. Cui, C. H. *et al.* Dystrophin conferral using human endothelium expressing HLA-E in the non-immunosuppressive murine model of Duchenne muscular dystrophy. *Hum Mol Genet* **20**, 235–244 (2011).
33. Selmani, Z. *et al.* HLA-G is a crucial immunosuppressive molecule secreted by adult human mesenchymal stem cells. *Transplantation* **87**, S62–S66 (2009).
34. Rouas-Freiss, N., Goncalves, R. M., Menier, C., Dausset, J. & Carosella, E. D. Direct evidence to support the role of HLA-G in protecting the fetus from maternal uterine natural killer cytolysis. *Proc Natl Acad Sci USA* **94**, 11520–11525 (1997).
35. Fernandez, N. *et al.* A critical review of the role of the major histocompatibility complex in fertilization, preimplantation development and feto-maternal interactions. *Hum Reprod Update* **5**, 234–248 (1999).
36. Pazmany, L. *et al.* Protection from natural killer cell-mediated lysis by HLA-G expression on target cells. *Science* **274**, 792–795 (1996).
37. Selmani, Z. *et al.* Human leukocyte antigen-G5 secretion by human mesenchymal stem cells is required to suppress T lymphocyte and natural killer function and to induce CD4 + CD25highFOXP3+ regulatory T cells. *Stem Cells* **26**, 212–222 (2008).
38. Hutter, H. *et al.* Expression of HLA class I molecules in human first trimester and term placenta trophoblast. *Cell Tissue Res* **286**, 439–447 (1996).
39. Paietta, E. Expression of cell-surface antigens in acute promyelocytic leukaemia. *Best Practice & Research Clinical Haematology* **16**, 369–385 (2003).
40. Gayoso, I. *et al.* Immunosenescence of human natural killer cells. *J Innate Immun* **3**, 337–343 (2011).
41. Fujimoto, M. & Sato, S. B cell signaling and autoimmune diseases: CD19/CD22 loop as a B cell signaling device to regulate the balance of autoimmunity. *J Dermatol Sci* **46**, 1–9 (2007).
42. Mafi, P., Hindocha, S., Mafi, R., Griffin, M. & Khan, W. S. Adult mesenchymal stem cells and cell surface characterization - a systematic review of the literature. *The Open Orthopaedics Journal* **5**, 253–260 (2011).
43. Han, K. *et al.* Human amnion-derived mesenchymal stem cells are a potential source for uterine stem cell therapy. *Cell Prolif* **41**, 709–725 (2008).
44. Nery, A. A. *et al.* Human mesenchymal stem cells: from immunophenotyping by flow cytometry to clinical applications. *Cytometry Part A* **83**, 48–61 (2013).
45. Kasprzak, A., Surdacka, A., Tomczak, M. & Konkol, M. Role of high endothelial postcapillary venules and selected adhesion molecules in periodontal diseases: a review. *J Periodontal Res* **48**, 1–21 (2013).
46. Elghetany, M. T. & Lacombe, F. Physiologic variations in granulocytic surface antigen expression: impact of age, gender, pregnancy, race, and stress. *J Leukoc Biol* **75**, 157–162 (2004).
47. Crisan, M., Corselli, M., Chen, W. C. W. & Péault, B. Perivascular cells for regenerative medicine. *J Cell Mol Med* **16**, 2851–2860 (2012).
48. Alakel, N. *et al.* Direct contact with mesenchymal stromal cells affects migratory behavior and gene expression profile of CD133+ hematopoietic stem cells during ex vivo expansion. *Exp Hematol* **37**, 504–513 (2009).
49. Dvorakova, J., Hruba, A., Velebny, V. & Kubala, L. Isolation and characterization of mesenchymal stem cell population entrapped in bone marrow collection sets. *Cell Biol Int* **32**, 1116–1125 (2008).
50. Mori, T. *et al.* Combination of hTERT and bmi-1, E6, or E7 induces prolongation of the life span of bone marrow stromal cells from an elderly donor without affecting their neurogenic potential. *Mol Cell Biol* **25**, 5183–5195 (2005).

Acknowledgments

We express our sincere thanks to Hatsune Makino, Kazumi Takanashi, Masanori Ihara, Tohru Sugawara, Yuichiro Harada, Yayoi Kajiwara, Tetsuo Maruyama, Hiroshi Uchida, Hirotaka Masuda, and other members of the National Research Institute for Child Health and Development and Keio University School of Medicine for valuable discussions and helpful advice. We also thank Kayoko Saito for secretarial work. This work was supported, in part, by a National Grant-in-Aid from the Japanese Ministry of Health, Labor, and Welfare (NCCHD24-6 to T.H. and H.A.), a Grant-in-Aid from the Japan Health Sciences Foundation (KHD1220 to T.H. and H.A.), and Grants-in-Aid from the Japan Society for the Promotion of Science (Kiban-C-23592413 to T.H. and Wakate-B-25861518 to K.S.).

Author contributions

K.S. and T.H. contributed to the experimental design, data acquisition, analysis and interpretation, and drafting of the article. M.Y., S.K. and S.O. provided technical support and assisted with the data analysis and interpretation. N.K., H.A., K.M., Y.Y. and A.U. assisted with experimental design as well as data analysis and interpretation. All authors examined the data and approved the final manuscript.

Additional information

Supplementary information accompanies this paper at http://www.nature.com/scientificreports

Competing financial interests: The authors declare no competing financial interests.

How to cite this article: Sugawara, K. *et al.* Derivation of human decidua-like cells from amnion and menstrual blood. *Sci. Rep.* **4**, 4599; DOI:10.1038/srep04599 (2014).

BASIC SCIENCE

Nanomedicine: Nanotechnology, Biology, and Medicine
10 (2014) 1165–1174

nanomedicine
Nanotechnology, Biology, and Medicine

ELSEVIER

Original Article

nanomedjournal.com

Pleiotropic functions of magnetic nanoparticles for *ex vivo* gene transfer

Daisuke Kami, PhD[a], Tomoya Kitani, MD[a], Tsunao Kishida, PhD[b], Osam Mazda, MD, PhD[b], Masashi Toyoda, PhD[c], Asahi Tomitaka, PhD[d], Satoshi Ota, MEng[e], Ryuga Ishii, PhD[f], Yasushi Takemura, PhD[e], Masatoshi Watanabe, MD, PhD[e], Akihiro Umezawa, MD, PhD[f], Satoshi Gojo, MD, PhD[a,*]

[a]*Department of Regenerative Medicine, Kyoto Prefectural University of Medicine, Kyoto, Japan*
[b]*Department of Immunology, Kyoto Prefectural University of Medicine, Kyoto, Japan*
[c]*Department of Vascular Medicine, Tokyo Metropolitan Institute of Gerontology, Tokyo, Japan*
[d]*Department of Materials Science and Engineering, University of Washington, Seattle, WA, USA*
[e]*Faculty of Engineering, Yokohama National University, Kanagawa, Japan*
[f]*Department of Reproductive Biology and Pathology, National Institute of Child Health and Development, Tokyo, Japan*

Received 17 October 2013; accepted 27 March 2014

Abstract

Gene transfer technique has various applications, ranging from cellular biology to medical treatments for diseases. Although nonviral vectors, such as episomal vectors, have been developed, it is necessary to improve their gene transfer efficacy. Therefore, we attempted to develop a highly efficient gene delivery system combining an episomal vector with magnetic nanoparticles (MNPs). In comparison with the conventional method using transfection reagents, polyethylenimine-coated MNPs introduced episomal vectors more efficiently under a magnetic field and could express the gene in mammalian cells with higher efficiency and for longer periods. This novel *in vitro* separation method of gene-introduced cells utilizing the magnetic property of MNPs significantly facilitated the separation of cells of interest. Transplanted cells *in vivo* were detected using magnetic resonance. These results suggest that MNPs play multifunctional roles in *ex vivo* gene transfer, such as improvement of gene transfer efficacy, separation of cells, and detection of transplanted cells.

From the Clinical Editor: This study convincingly demonstrates enhanced efficiency of gene transfer via magnetic nanoparticles. The method also enables magnetic sorting of cells positive for the transferred gene, and in vivo monitoring of the process with MRI.

Key words: Episomal vector; *Ex vivo* gene transfer; *In vitro* cell separation; Magnetic nanoparticles; Magnetic resonance imaging

Nanotechnology describes the creation and utilization of materials, devices, and systems with nanometer-sized scaffolds that are applied in fields such as physics, chemistry, biology, engineering, materials science, and medicine.[1] Nanoparticles are generally defined as particles of approximately 1-100 nm; this size range is similar to that of several proteins and nucleic acids. In particular, intensive efforts are underway to develop nanomaterials for ideal pharmaceutical agents specific to a target organ, tissue, or cell. Nanomedicine refers to the medical application of nanotechnology in the monitoring, diagnosis, prevention, and treatment of various diseases, which is currently revolutionizing modern medicine.[2] Several clinical trials using nanocarriers loaded with anticancer drugs and RNAs for gene silencing are underway to treat several types of cancer.[3]

Till date, several delivery systems using nanoparticles in combination with nucleic acids and chemical drugs have been reported.[4-6] Magnetic nanoparticles (MNPs) opened a novel avenue for integrative therapeutics and diagnostic applications, which is known as nanotheranostics.[2] The attraction of MNPs toward an external magnetic field has been exploited for purposes such as delivering genes or drugs to target sites and

We express our sincere gratitude to M. Nakata (Kyoto Prefectural University of Medicine, Kyoto, Japan) for contributing toward cell culture and FACS analysis.

Funding: This study was supported by a Grant-in-Aid for the Science for Future Molecular Systems from the Ministry of Education, Culture, Sports, Science and Technology, Japan (MEXT).

Conflict of Interest: The authors report no conflicts of interest in this work. The authors have no financial interests or conflicts with regard to the subject matter discussed in this manuscript.

*Corresponding author at: Department of Regenerative Medicine, Kyoto Prefectural University of Medicine, Kyoto, Japan.

E-mail address: gojos@koto.kpu-m.ac.jp (S. Gojo).

http://dx.doi.org/10.1016/j.nano.2014.03.018
1549-9634/

tracing cells by magnetic resonance imaging (MRI).[7] MNPs have been used as adjuvants to improve gene transfer efficacy by up to several 100-fold under a magnetic field. Magnetic gene transfer is defined as "magnetofection".[8] Magnetofection has been combined with either nonviral[9] or viral vectors including retrovirus,[10] adenovirus,[11] and adeno-associated virus.[12] In the mechanism of magnetofection, magnetic forces may accelerate the sedimentation of the complex between MNPs and DNAs or viral vectors onto the cell surface and not enforce endocytosis into the cell.[13] Although there is a concern regarding nanotoxicity owing to the greatly enhanced reactive surface area of nanoparticles, their ability to cross cell membranes, and their resistance to biodegradation, which may result in apoptosis and genotoxicity via inflammatory responses,[14] their advantages such as improving the dose–response relationship and kinetics of nucleic acid delivery are pushing the methodology toward the clinical arena.

In our laboratory, as previously described, we have developed a gene delivery system using iron oxide (γ-Fe_2O_3) MNPs and magnetic force.[15,16] To efficiently increase gene delivery, we focused on cationic polymer deacylated polyethylenimine (PEI) and PEI-coated MNPs (PEI-MNPs) that are capable of interacting with nucleic acids. PEI-MNPs form complexes with nucleic acids (e.g., plasmids), called magnetoplexes, in water.[15] They are efficiently introduced into cells by a magnetic field produced by a magnetic plate under the culture dish. PEI-MNPs have been reported to show dramatically decreased cytotoxicity compared with uncoated nanoparticles,[17] and iron oxide has already been used in clinical applications as a contrast agent for MRI.[18]

However, there is still a serious concern about the genomic integration of exogenous genes, which may result in carcinogenesis and ectopic differentiation. Therefore, a transient gene transfer system is required, particularly for clinical applications. For the same reason, several protocols involving the use of episomal vector plasmids,[19,20] Sendai virus,[21] and synthesized mRNA[22] have been reported. However, these methods are much less efficient than the retrovirus method. A gene transfer system using an episomal vector was adopted as a standard protocol to generate induced pluripotent stem cells (iPSCs) for human cell banking in Japan. The episomal vector constructed by Mazda et al[19] comprised the Epstein–Barr (EB) virus antigen-1 (*EBNA-1*) gene and *OriP* sequence placed in the backbone of a construct with artificial chromosome-like characteristics such as cytoplasm-to-nuclear transport, nuclear retention, and replication and segregation of the DNA. Insertion of the *EBNA-1* gene and *OriP* sequence into recombinant plasmid DNA, the so-called episomal vector, may allow the replication and maintenance of the plasmid in mammalian cells. We accordingly examined whether the gene delivery system combined with an episomal vector and modified PEI-MNPs could reinforce the gene transfection efficacy using a novel *in vitro* cell separation procedure based on the magnetic property of PEI-MNPs themselves without any additional magnetic materials.

Methods

Experimental procedures

Details of quantitative reverse transcription PCR (qRT-PCR), flow cytometric analysis, inductively coupled plasma mass spectrometry (ICP-MS), cell viability, MRI, pathohistological analysis, and statistical analysis are provided in the Supplementary Document.

Materials

MNPs (γ-Fe_2O_3) were purchased from CIK NanoTek (Tokyo, Japan). Deacylated PEI, PEI max linear (MW 25,000), was purchased from Polysciences, Inc. (Warrington, PA, USA). Deionized water was purchased from Life Technologies, Corp. (Carlsbad, CA, USA). Magnetic plate (1.2 T) was purchased from OZ Biosciences Inc. (Marseille, France). Episomal vector was provided by T.K. and O.M. (Supplementary Figure 1).

Preparation of PEI-MNPs

PEI-MNPs were prepared as reported in previous reports[15,16] (Supplementary Figure 2). In brief, MNPs (1.0 g) were dissolved in 30 ml PEI solution (1.6 mg PEI/ml). The mixture was sonicated for 2 min at 40 W on ice, and 20 ml of deionized water was then added (final concentration, 1.0 mg PEI/ml). The ferrofluid was centrifuged at 4,100 $\times g$ for 5 min, and subsequently, the supernatant was transferred into fresh tubes. The fluids were washed twice with deionized water and dissolved into equal volumes of PEI solution (1.0 mg PEI/ml) to prevent agglomerations. MNPs in this fluid were coated with PEI and dispersed (PEI-MNPs). The diameter of PEI-MNPs was approximately 120 nm as deduced using laser light scattering method.[16]

Mouse embryonic fibroblast (MEF) isolation, cell culture, and MNP transfection

Experimental procedures and protocols were approved by the Animal Experiment Ethics Committee of the Kyoto Prefectural University of Medicine. For MEF isolation, uteri removed from 13.5-day pregnant C57/B6 mice were washed using phosphate-buffered saline (PBS; Wako Pure Chemical Industries, Ltd., Osaka, Japan). The head and visceral tissues were removed from isolated embryos. The remaining bodies were washed using fresh PBS, minced with scissors, and transferred into fresh Dulbecco's modified Eagle's medium (DMEM; Wako Pure Chemical Industries, Ltd.) supplemented with 10% fetal bovine serum (FBS) and 1% penicillin and streptomycin (Life Technologies, Corp.). Three days after incubation, outgrowth cells were trypsinized, collected by centrifugation (200 $\times g$ for 5 min), and resuspended in fresh medium. Following the first passage, 1×10^6 cells were cultured in 150-mm dishes at 37 °C under 5% CO_2. In this study, we used MEFs within 3-5 passages. MEFs were cultured using DMEM containing 10% FBS and 1% penicillin and streptomycin at 37 °C under 5% CO_2. To perform transfection using episomal GFP vector, 1×10^5 MEFs were plated in each well of a 6-well plate a day before transfection. Immediately before transfection, cells were rinsed and supplemented with 1 ml of fresh culture medium. PEI-MNPs (7.5 μl, 0.05 mg PEI-MNPs in 1 mg PEI/ml) were mixed with 2.5 μg episomal vector (pEF.OriP9.GFP.E.) and incubated in deionized water at a final volume of 50 μl at room temperature for 15 min. The complexes were then added to the MEF culture dishes placed on a magnetic plate for 4 h. PEI (7.5 μl) solution (1 mg PEI/ml, without MNPs) was used as a control. The medium was

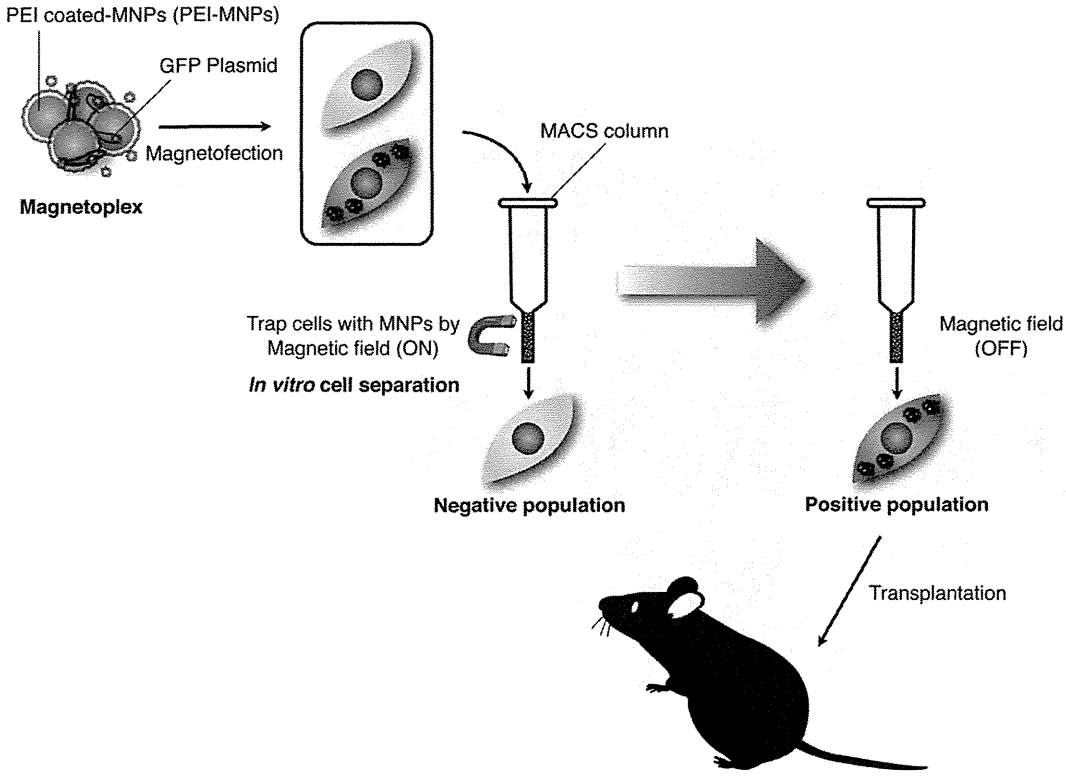

Figure 1. Schema of the experiment.First, PEI-MNPs containing the episomal plasmid (i.e., magnetoplex) were transferred into the cells. Second, *in vitro* cell separation was performed as illustrated at the center of figure. Cells containing the magnetoplex, which has a net magnetization, were enriched using an MACS column and a magnetic field. Third, the positive population was transplanted into the legs of mice.

replaced with fresh DMEM supplemented with 10% FBS 4 h after MNP transfection, and the cells were cultivated for subsequent experiments.

In vitro cell separation by PEI-MNPs

Two days after transfection, transfected MEFs were harvested by trypsin treatment and resuspended into 0.5 ml autoMACS running buffer (Miltenyi Biotec KK, Bergisch-Gladbach, Germany). The cell solution was loaded into a magnetic-activated cell sorting (MACS) MS column (Miltenyi Biotec KK) under a magnetic field. The column was washed thrice using autoMACS buffer to elute MEFs that did not contain PEI-MNPs; these were considered to be non-transfected and were designated as the negative population of cells (Figure 1). The cells retained in the column under the magnetic force, which were expected to be gene-transfected cells, were flushed out with autoMACS buffer using a plunger supplied with the column; these cells were designated as the positive population of cells (Figure 1). Subsequent to this *in vitro* step, the enriched cells were seeded in a 6-well culture plate for 5 days at 37 °C under 5% CO_2.

Results

Episomal vector transfection efficiency was increased by PEI-MNPs

Episomal vector transfection efficiency in the presence of PEI-MNPs (PEI-MNPs with magnetic field group) was compared with the PEI transfection method (PEI group) or PEI-MNPs without placing on the magnetic plate (PEI-MNPs without magnetic field group). Using fluorescence microscopy, we detected more GFP-positive cells using PEI-MNPs with magnetic field than those using PEI or PEI-MNPs without magnetic field (Figure 2, *A*). To evaluate the transfection efficiency, qRT-PCR (Figure 2, *B*) and flow cytometric analysis (Figure 2, *C*) were performed at days 2, 4, and 7 after transfection. GFP expression level in the PEI-MNPs with magnetic field group was increased by approximately 6-8-fold (Figure 2, *B*), and the expression in MEFs was sustained for 7 days (Figure 2, *C*) in comparison with that in the PEI group. Both the relative GFP expression level and the GFP-positive cell ratio to the complete cell number decreased with time in the PEI-MNPs with magnetic field group. The decrease in the relative GFP expression level was consistent with that in other studies using the same episomal vector[19]; further, the levels in the PEI or PEI-MNPs without magnetic field groups were too low to allow estimation of a time trend (Figure 2, *B*). The reduction rate of GFP positive ratio in PEI, and PEI-MNPs without, or with magnetic field on day 7, compared with GFP positive cell ratio in each group on day 2, were 43.6%, 20.5%, and 42.7%, respectively, which were not significant different based on ordinary one-way ANOVA (Figure 2, *C*).

Cell characterization after in vitro cell separation

We successfully developed a novel *in vitro* separation method for transfected cells containing PEI-MNPs using a

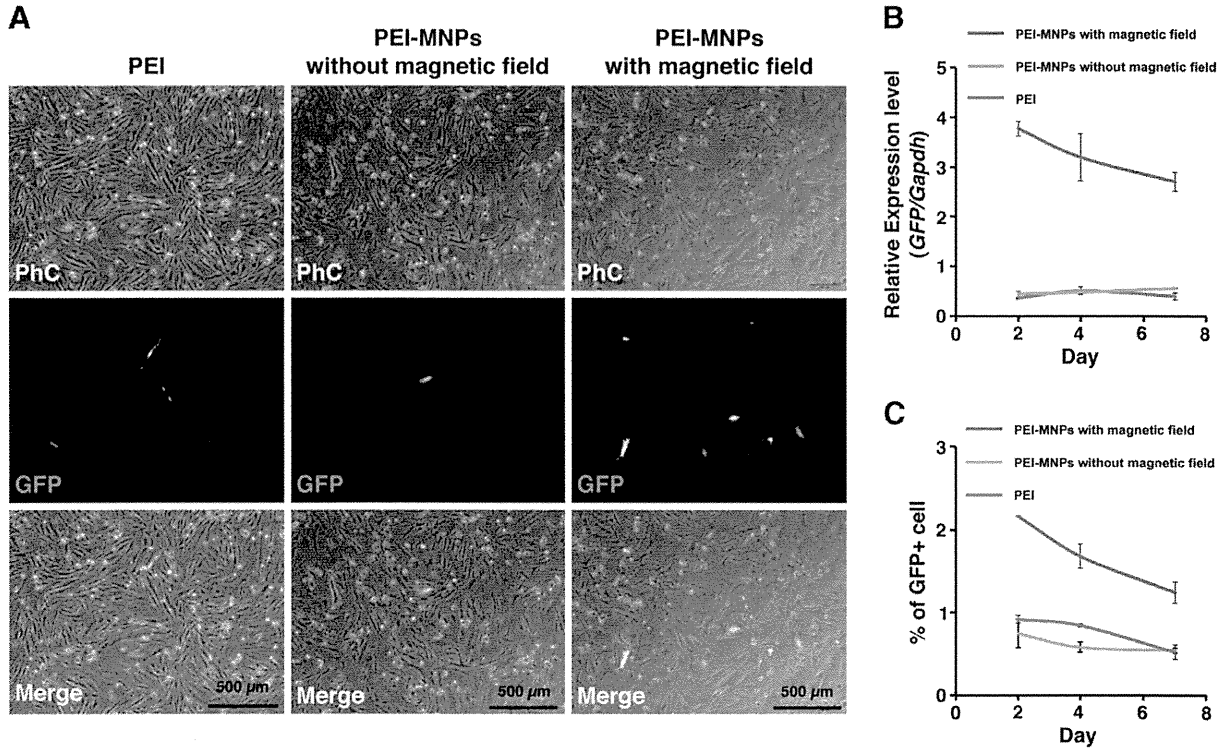

Figure 2. Efficient transfection method using magnetic nanoparticles (MNPs) and an episomal vector.**(A)** Phase contrast fluorescence microscopy images. Mouse embryonic fibroblasts (MEFs) were transfected with episomal vector pEF.OriP9.GFP.E. and polyethylenimine (PEI)-coated MNP (PEI-MNPs) with magnetic field. Transfections with PEI or with PEI-MNPs without magnetic field were used as controls. Black bar indicates 500 μm; PhC, phase contrast. **(B)** qRT-PCR of GFP expression in MEFs using PEI, PEI-MNPs with magnetic field, or PEI-MNPs without magnetic field. Individual RNA expression levels were normalized to the respective mouse *Gapdh* expression levels. pCAGGS-GFP plasmid-transfected MEFs were used as a reference. Error bars indicate SE (n = 4). **(C)** Flow cytometric analysis of GFP-positive MEFs treated with PEI, PEI-MNPs with magnetic field, or PEI-MNPs without magnetic field. All results were compared with non-transfected cells. Error bars indicate SE (n = 3).

magnetic field and MACS column (*in vitro* cell separation) (Figure 1). We evaluated the total iron content per cell, cell viability, and GFP-positive cell percentage of PEI-MNP-transfected MEFs in the time course depicted in Figure 3, *A*. First, we measured the total iron content per cell using ICP-MS. The total iron content per unenriched MEF remained approximately the same from days 2 to 14 (Figure 3, *B*). In addition, the total iron content per MEF at day 2 in the positive population was 3.12 ± 0.60 pg/cell (expressed as mean ± standard error), whereas that in the negative population was 0.14 ± 0.05 pg/cell; the total iron content per MEF before the procedure was 0.56 ± 0.10 pg/cell (Figure 3, *C*). In comparison with the negative population, the positive population exhibited an approximately 23-fold increase in the total iron content. In addition, the number of PEI-MNPs in the positive and negative populations was calculated to be $22.4 \pm 4.31 \times 10^3$ and $1.0 \pm 0.36 \times 10^3$ MNPs/cell, respectively (Figure 3, *D* and Supplementary Figure 3). We measured cell viability after separation at days 2 and 7. Although the enriched cell viability on day 2 was 38% ± 8.9%, the viability on day 7 recovered to 83% ± 8.6% (Figure 3, *E*). This poor cell viability of the positive population was attributed to excessive genetic material within the cells, because the viability of the positive population in a mock experiment, which was performed without the episomal vector, was similar to that of the control (Supplementary Figure 4). The percentage of PEI-MNP-transfected cells was too low to influence the cell viability of the entire population, and there was no significant difference between the entire cell population prior to the enrichment and the negative population with regard to cell viability (Figure 3, *E*). The absolute cell number at days 2 and 7 and the doubling times during this period for both the populations following the *in vitro* separation procedure were plotted (Figure 3, *F* and *G*). The growth properties were not significantly influenced by the separation procedure. The number of cells in the positive population was 2.9×10^4 and the doubling time was 3.28 days; the number of cells and doubling time were similar to the cells that were only transfected and to those in the negative population.

Efficacy of in vitro cell separation

To evaluate the efficacy of *in vitro* cell separation, we compared the expression of GFP in the gene-transfected cells without *in vitro* cell separation (Figure 4, *A*) with that those with *in vitro* cell separation (Figure 4, *B*) using fluorescence microscopy. Because the cell viability in the positive population was approximately 38%, the cell number was less than that prior to the separation procedure. Although as per the fluorescent images, the positive population was not enriched for exogenous gene expression, the merged views reveal the sparseness of cells after the procedure, and the ratio of the positive population to the entire cell population was judged to be higher than that without the

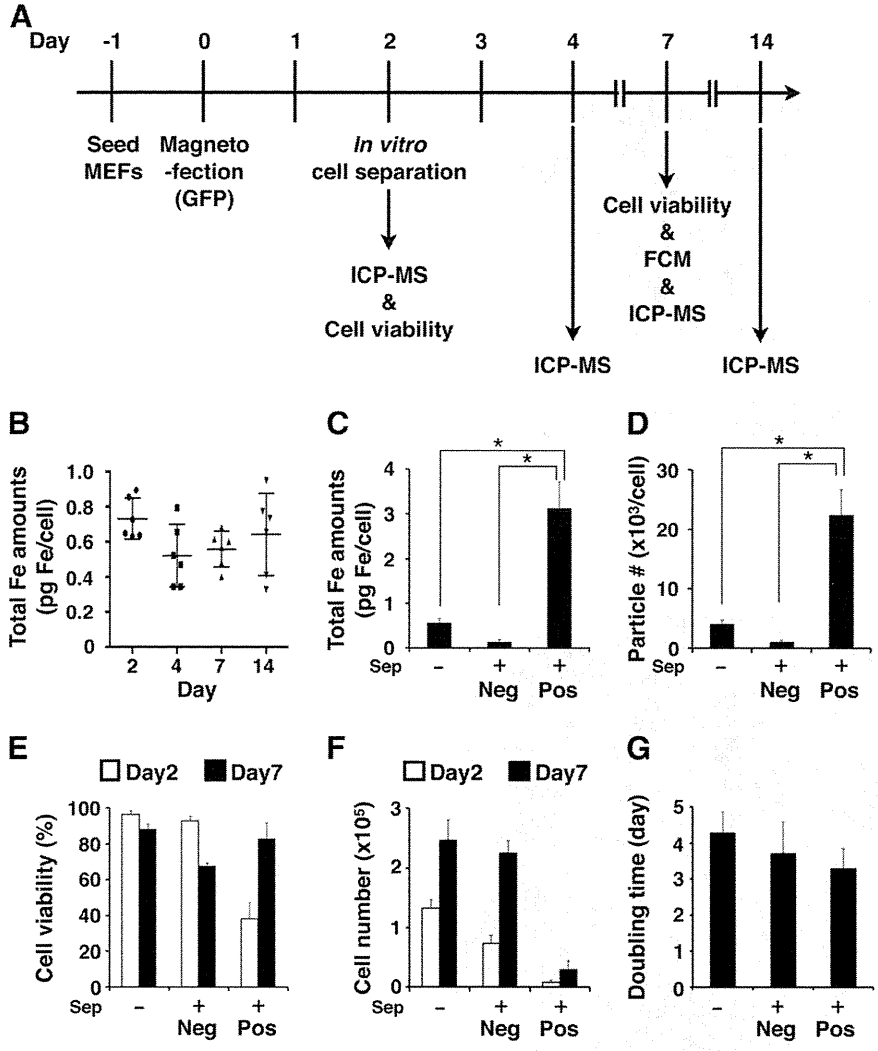

Figure 3. Evaluation of the total iron content per cell and cell viability by *in vitro* cell separation. **(A)** Time course for evaluating *in vitro* cell separation. MEFs were analyzed by ICP-MS, cell viability assay, and flow cytometric analysis. Medium was replaced every 2 or 3 days. **(B** and **C)** Inductively coupled plasma-mass spectrometer (ICP-MS) was used to measure iron uptake by MEFs. The total iron content was corrected according to cell number. Error bars indicate SE; * indicates statistical significance ($P < 0.05$). Time-dependent changes in the total iron content per unenriched MEF were approximately the same from days 2 to 14 **(B)**. Two days after transfection, MEFs containing PEI-MNPs were enriched by a magnetic field **(C)**. **(D)** The number of MNPs in MEFs was calculated (Supplementary Figure 3). **(E)** Cell viability was examined at days 2 and 7 following gene transfer. Pos and Neg represent the positive and negative populations for *in vitro* cell separation, respectively. **(F)** Cell number in both fractions after *in vitro* cell separation. **(G)** Doubling times in both the groups were approximately the same. Sep represents *in vitro* cell separation.

enrichment (Figure 4, *A* and *B*). Figure 4, *C* demonstrates the representative density plot analysis by flow cytometer. The percentages of GFP-positive cells as the average of the experimental series without and with the separation procedure were 3.7% and 8.4%, respectively; the enrichment ratio was approximately 2.3-fold (Figure 4, *D*). We calculated the total number of GFP-positive cells in both the positive and negative populations 7 days after gene transfer. The sensitivity and specificity were 82.65% ± 1.51% and 59.68% ± 0.55%, respectively. We repeated the separation procedure to determine whether the number of GFP-positive cells increased upon sequential *in vitro* cell separation. The average number of viable cells on day 2 following second enrichment decreased to 2.0×10^4 from 2.42×10^4, which were acquired following the first enrichment. The GFP-positive cell ratio on day 7 following second enrichment also decreased to 6.5% from 8.9% (Figure 4, *C*). To compare our procedure with a standard protocol involving an episomal vector for human iPSCs, electroporation was performed (Supplementary Figure 5). The total number of GFP-positive cells was 6.27×10^2 cells 7 days after electroporation, while it was 2.4×10^3 cells in the positive population 7 days after *in vitro* cell separation using PEI-MNPs (Figures 3, *F* and 4, *D* and Supplementary Figure 5).

MRI analysis of PEI-MNP-enriched cells in mice

Compared with the absence of signals in the control sample (Figure 5, *A* and *B*), GFP gene-transfected MEFs could be

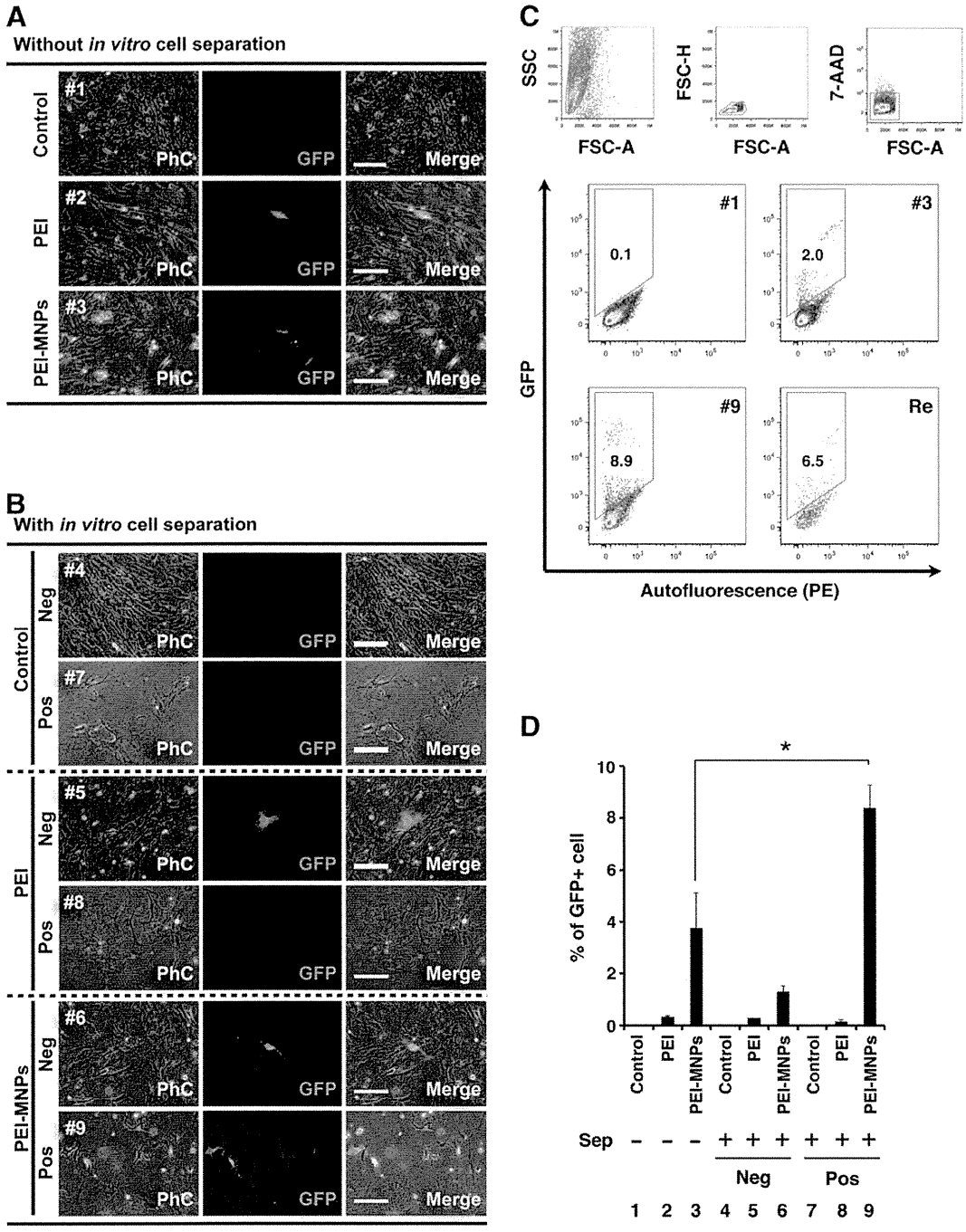

Figure 4. Efficacy of *in vitro* cell separation by fluorescent microscopy and flow cytometric analysis.**(A** and **B)** Phase contrast fluorescence microscopy images of GFP-transfected MEFs 7 days after transfection without *in vitro* cell separation **(A)** and with separation **(B)**. White bar indicates 500 μm. Numbers listed in each phase contrast image (PhC) in **(A)**, **(B)**, and **(C)** correspond to the numbers in the graph **(D)**. **(C)** Representative flow cytometric analysis of GFP-positive MEFs treated with PEI or PEI-MNPs. Three figures in the upper row (FSC-A vs. SSC, FSC-A vs. FSC-H, and FSC-A vs. 7-AAD) reveal sample gating. The remaining 4 figures [autofluorescence (PE) vs. GFP] represent each sample [the numbers correspond to those in **(A)**, **(B)**, and **(D)**]. Re indicates the sequential re-separation of MNPs. **(D)** The plot at the bottom right shows the percentage of GFP-positive MEFs in each condition analyzed by flow cytometric analysis. All results were compared with non-transfected cells as a control. Error bars indicate SE (n = 3-5); * indicates statistical significance ($P < 0.05$).

clearly detected with MRI at the point of transplantation corresponding to the injection site (Figure 5, *C*, white arrowhead) immediately after implantation on day 7. The signal intensity of the grafts slightly decreased but did not migrate to other parts of the body.

Pathohistological analysis

The quadriceps femoris muscle was dissected after MRI measurement on day 7 for pathohistological analyses. Prussian blue staining, which targets iron, clearly revealed positive cells

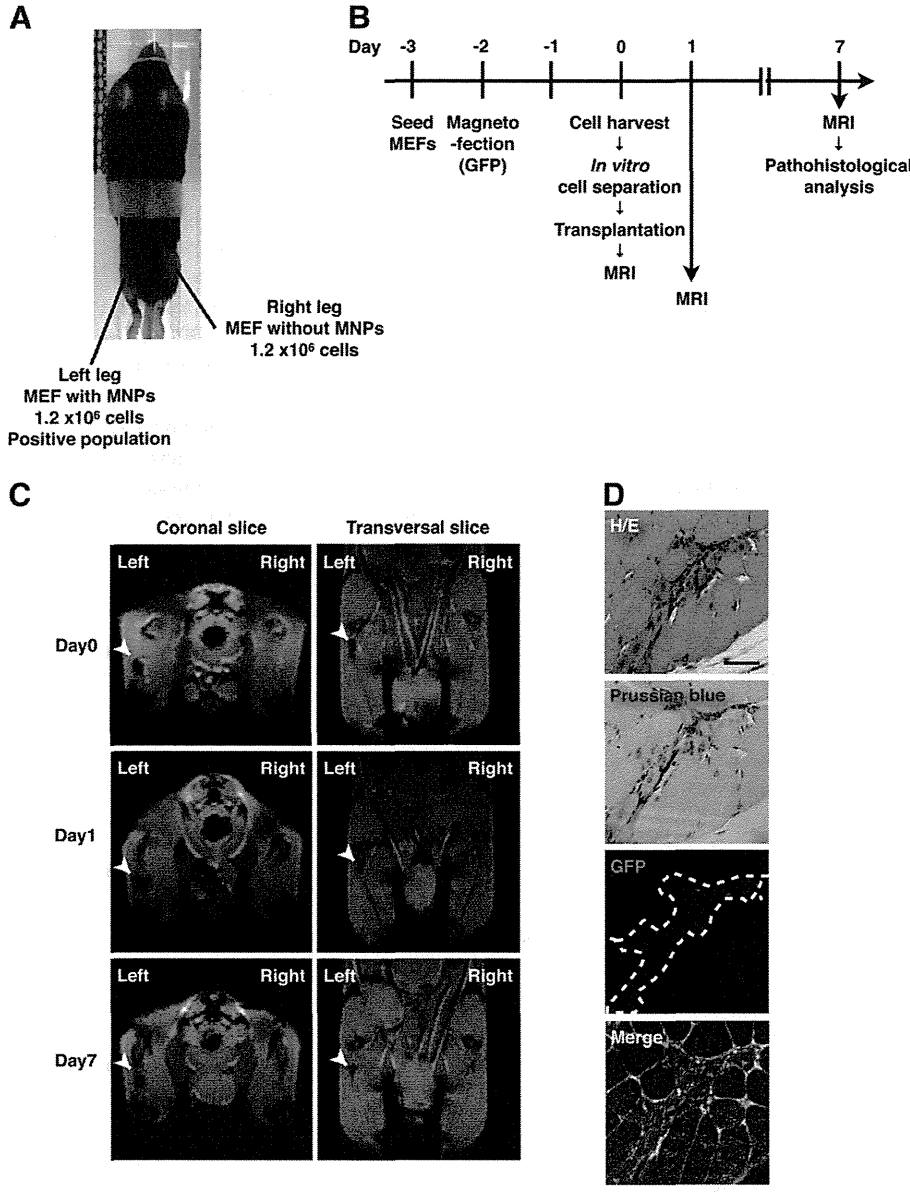

Figure 5. *In vivo* MRI measurements using MNP-transfected and -enriched MEFs. **(A)** Posture of the anesthetized mouse at MRI scans. The right leg was injected with MEFs without treatment. The left leg was injected with the positive population for *in vitro* cell separation. **(B)** Schematic illustration of the experimental design for *in vivo* MRI measurements using PEI-MNP-transfected and -enriched MEFs. **(C)** After intramuscular injection in the legs of C57/B6 mice, sequences of 4.7-T magnetic resonance images were obtained at days 0, 1, and 7 in the coronal and transversal planes. The GFP-transfected MEFs were injected into the left leg, whereas the untreated MEFs were injected into the right leg. **(D)** Pathohistological analysis of transplantation of GFP-transfected MEFs at day 7 in the injected leg by hematoxylin–eosin (H&E) and Prussian blue staining and immunohistochemical staining with anti-GFP. Black bar indicates 50 μm.

corresponding to MRI-positive sites (Figure 5, *D*). Using immunofluorescence staining with GFP antibody, GFP-positive cells in tissue sections indicated that PEI-MNP-transfected cells were viable. No inflammatory cells were identified in the equivalent areas of the histology specimen.

Discussion

Here we report that in addition to their previously reported dual roles in aiding gene transfer and cell tracing, PEI-MNPs coupled with an episomal vector can successfully enable *in vitro* cell separation.

Gene delivery techniques enable the introduction of a gene of interest in host cells to express the corresponding encoded protein either *in vivo* or *in vitro*. At present, there are 3 primary gene delivery systems that employ viral vectors (e.g., retroviruses and adenoviruses), nucleic acid electroporation, and nucleic acid transfection. Their efficacy and cytotoxicity depend on their machinery for transferring genes into target cells. Although gene delivery by viral vectors generally exhibits high efficiency, these methods have some drawbacks, such as

genomic insertions in retroviruses and exogenous gene dilution in adenoviruses.[23] Although electroporation is efficient for introducing exogenous genes into host cells, its cytotoxicity as a result of electrical stimulation cannot be estimated.[24] Transfection reagents, such as PEI and lipofectamine, can form complexes with plasmid DNAs (i.e., polyplexes), causing inefficient delivery of plasmid DNAs into target cells. However, cell viability is largely preserved and this method is safe for clinical use. Therefore, this method is relatively more promising than others for medical applications, provided its efficiency is improved. Many scientists have already reported the use of MNPs in basic research to increase the transfection efficiency of cultivated cells.[8-13,15,16,25] However, the mechanism of MNP gene delivery and gene expression is not yet completely understood; it has still not been optimized for clinical applications, and here, we have discussed the following 3 issues: cellular uptake, endosomal escape, and cytotoxicity.

The uptake of nanoparticles by cells occurs via several mechanisms, which comprise passive transport and active endocytosis; the latter is further classified into nonspecific and receptor-mediated endocytosis.[26] Magnetoplexes and polyplexes are reportedly internalized via caveolae- or clathrin-mediated endocytosis.[25,27-29] The uptake of these complexes is limited by size (up to hundreds of nanometer). The influence of the size of nanoparticles on endocytosis has been investigated using poly(D,L-lactide-co-glycolide) nanoparticles fractionated into small (<100 nm) and large (>100 nm) sizes,[30] gold nanoparticles stratified to 45, 70, and 110 nm,[31] and latex fluorescent beads of defined size (50-1,000 nm).[32] These studies showed that a high rate of cellular internalization could be achieved with smaller-sized nanoparticles. Other research groups, including ours, have previously tested several types of PEI as a coating material for gene transfer, showing that a linear type of 25-kDa PEI was the optimal for γ-Fe_2O_3.[16,33,34] Moreover, we reported that the size limitation for endocytosis using the same nanoparticles with DNA plasmids was <500 nm.[25] Using an *N*-alkyl-PEI2k coating modification on MNPs, the average nanoparticle size was 54.7 ± 9.5 nm, with less cytotoxicity.[35] Cell-penetrating peptides, including low-molecular weight protamines[36] and Tat peptide,[37] have also been demonstrated to be capable of translocating conjugated materials into cells, regardless of their size or hydrophilicity. These surface coatings should effectively support the engulfment of nanoparticles by cells. To enhance the efficiency of gene delivery using MNPs, it is important to control the size of MNPs and their complexes. In this study, we used nonuniformly sized PEI-MNPs (Supplementary Figure 2); therefore, establishment of a method for synthesizing uniformly sized PEI-MNPs should enhance their gene transfection efficiency.

Exogenous materials internalized via endocytosis are engulfed into endosomes, which eventually become lysosomes, where enzymatic decay processes occur.[38] This physiological reaction may be related to the reduced expression of GFP. To circumvent this decay, the release of cargos into the cytosol prior to endosomal escape ameliorates gene expression during gene transfer. Several mechanisms have been proposed to achieve this aim, including pore formation in the endosomal membrane, pH-buffering effect (also known as the proton sponge effect) in the case of PEI,[39] fusion with the endosomal membrane, and photochemical disruption of the endosomal membrane. Some synthetic endosomolytic peptides such as arginine-rich cell penetrating peptides[40] and an analogue of glycoprotein H from herpes simplex virus[41] have been reported to enhance gene expression. The latter approach has been reported to increase the expression levels in human cells by up to 30-fold. Thus, a combination of an endosomal escape agent with this system may potentially reach a clinical stage.[42]

We previously reported that a variety of ferrite nanoparticles, such as Fe_3O_4, $CoFe_2O_4$, $MgFe_2O_4$, and $NiFe_2O_4$, were characterized with regard to their magnetic properties and cytotoxicity in cultured human cells.[43] For striking a balance between magnetization and biocompatibility, Fe_3O_4 could be a suitable agent for gene transfer. In this study, γ-Fe_2O_3 was used, which has properties similar to those of Fe_3O_4. Although PEI modifications can be executed onto each nanoparticle, other nanoparticles may be less balanced. At present, superior coating materials are being developed, such as low molecular weight alkyl-polycation,[35] cationic stearic acid-grafted PEI copolymers and anionic poly(ethylene glycol)-poly(γ-benzyl-L-glutamate),[44] aminodextran, 3-aminopropyltriethoxysilane, and dimercaptosuccinic acid.[45] These reagents can be combined to produce nanoparticles with high magnetization but lower biocompatibility, although they may improve the separation efficacy with negligible cytotoxicity.

The major gene delivery method of episomal vectors is currently electroporation. However, this method does not guarantee a high efficacy of gene transfer, which was only 10%-20% in our experiment. When we attempted to increase the efficacy of gene transfer in electroporation, the cytotoxicity also increased, resulting in cell death. Poor gene transfer efficacy and high cytotoxicity correspond to the size of episomal vectors. Episomal vectors generally contain a promoter sequence, target cDNA sequence, *EBNA-1* sequence of approximately 2,000 bp, *OriP* sequence of approximately 2,200 bp, and drug-resistant genes; these elements contribute to their large size. The size of an episomal vector without target cDNA may exceed 8,000 bp. PEI-MNPs can easily bind to episomal vectors through electrostatic interaction.[46] In a previous study, we demonstrated that the addition of PEI-MNPs could improve plasmid gene transfer.[16] In this study, in comparison with the conventional transfection reagent method, we succeeded in developing a more efficient transfection method using episomal vectors. Although an approximately 2-fold increase in efficacy was achieved, our new strategy resulted in a transfection efficiency of only 2%. However, we established a novel procedure to enrich cells containing PEI-MNPs *in vitro*. To the best of our knowledge, this is the first report to demonstrate that PEI-MNPs themselves could drive PEI-MNP-containing cells and express an exogenous gene under the influence of magnetic field *in vitro*; however, the concept of MNPs themselves driving cells under magnetic field has been previously presented.[47] Further, although the sensitivity of our novel procedure was satisfactory, the specificity remains to be improved, i.e., the separation procedure needs to be improved as the positive population that passed through the magnetic field contained a significant proportion of the negative population. Given the more powerful magnetic properties of

MNPs or stronger magnetic fields through the column or both,[43] could be the purification, not incomplete enrichment. Our protocol could successfully overcome the shortcomings of the large EB virus vector, including poor gene transfer efficacy and high cytotoxicity.

Cell separation by FACS and MACS[48,49] has been widely used in basic and clinical fields. FACS and MACS are used for the separation of heterogeneous cell populations according to their surface antigens or expression of fluorescent proteins in the cell. However, almost all the antibodies used for FACS and MACS are xenogeneic antibodies, which may cause immunological responses in case of cell transplantation. This *in vitro* cell separation was achieved owing to the attraction property of MNPs themselves within the cells under a magnetic field. Our method does not require a cumbersome fluorescent protein inside the cells, fluorescent-conjugated antibody targeting specific cell surface antigens, or additional magnetic materials. We expect that it will become a new strategy for *in vitro* cell separation. Thus, *in vitro* cell separation coupled to gene transfer through the EB virus vector should become a standard procedure for *ex vivo* gene transfer, particularly in case of direct conversion, which is defined as an alteration in cell fate of terminally differentiated cells via intervention of transcriptional networks.[50]

In this study, using *in vitro* and *in vivo* experiments, we demonstrated a novel multifactorial magnetofection achieved by transfection using PEI-MNPs and an *in vitro* cell separation and enrichment using a magnetic field. Magnetofected cells could be clearly detected around the point of transplantation corresponding to the injection site for a week. Our results suggest that MNP separation using PEI-MNPs should lead to new possibilities not only as transfection reagents but also as separating reagents and contrast agents for MRI. Although further improvements are warranted, this will be a novel strategy for *ex vivo* gene transfer for clinical applications.

Appendix A. Supplementary data

Supplementary data to this article can be found online at http://dx.doi.org/10.1016/j.nano.2014.03.018.

References

1. Leszczynski J. Bionanoscience: nano meets bio at the interface. *Nat Nanotechnol* 2010;**5**(9):633-4.
2. Mura S, Couvreur P. Nanotheranostics for personalized medicine. *Adv Drug Deliv Rev* 2012;**64**(13):1394-416.
3. Kim BY, Rutka JT, Chan WC. Nanomedicine. *N Engl J Med* 2010;**363**(25):2434-43.
4. Hrkach J, Von Hoff D, Mukkaram Ali M, Andrianova E, Auer J, Campbell T, et al. Preclinical development and clinical translation of a PSMA-targeted docetaxel nanoparticle with a differentiated pharmacological profile. *Sci Transl Med* 2012;**4**(128):128ra39.
5. Davis ME, Zuckerman JE, Choi CH, Seligson D, Tolcher A, Alabi CA, et al. Evidence of RNAi in humans from systemically administered siRNA via targeted nanoparticles. *Nature* 2010;**464**(7291):1067-70.
6. Govindarajan S, Kitaura K, Takafuji M, Ihara H, Varadarajan KS, Patel AB, et al. Gene delivery into human cancer cells by cationic lipid-mediated magnetofection. *Int J Pharm* 2013;**446**(1–2):87-99.
7. Li XX, Li KA, Qin JB, Ye KC, Yang XR, Li WM, et al. In vivo MRI tracking of iron oxide nanoparticle-labeled human mesenchymal stem cells in limb ischemia. *Int J Nanomedicine* 2013;**8**:1063-73.
8. Scherer F, Anton M, Schillinger U, Henke J, Bergemann C, Kruger A, et al. Magnetofection: enhancing and targeting gene delivery by magnetic force in vitro and in vivo. *Gene Ther* 2002;**9**(2):102-9.
9. Mykhaylyk O, Antequera YS, Vlaskou D, Plank C. Generation of magnetic nonviral gene transfer agents and magnetofection in vitro. *Nat Protoc* 2007;**2**(10):2391-411.
10. Hughes C, Galea-Lauri J, Farzaneh F, Darling D. Streptavidin paramagnetic particles provide a choice of three affinity-based capture and magnetic concentration strategies for retroviral vectors. *Mol Ther* 2001;**3**(4):623-30.
11. Pandori M, Hobson D, Sano T. Adenovirus-microbead conjugates possess enhanced infectivity: a new strategy for localized gene delivery. *Virology* 2002;**299**(2):204-12.
12. Mah C, Fraites Jr TJ, Zolotukhin I, Song S, Flotte TR, Dobson J, et al. Improved method of recombinant AAV2 delivery for systemic targeted gene therapy. *Mol Ther* 2002;**6**(1):106-12.
13. Huth S, Lausier J, Gersting SW, Rudolph C, Plank C, Welsch U, et al. Insights into the mechanism of magnetofection using PEI-based magnetofectins for gene transfer. *J Gene Med* 2004;**6**(8):923-36.
14. Nel A, Xia T, Madler L, Li N. Toxic potential of materials at the nanolevel. *Science* 2006;**311**(5761):622-7.
15. Kami D, Takeda S, Itakura Y, Gojo S, Watanabe M, Toyoda M. Application of magnetic nanoparticles to gene delivery. *Int J Mol Sci* 2011;**12**(6):3705-22.
16. Kami D, Takeda S, Makino H, Toyoda M, Itakura Y, Gojo S, et al. Efficient transfection method using deacylated polyethylenimine-coated magnetic nanoparticles. *J Artif Organs* 2011;**14**(3):215-22.
17. Zhang H, Xia T, Meng H, Xue M, George S, Ji Z, et al. Differential expression of syndecan-1 mediates cationic nanoparticle toxicity in undifferentiated versus differentiated normal human bronchial epithelial cells. *ACS Nano* 2011;**5**(4):2756-69.
18. Arbab AS, Liu W, Frank JA. Cellular magnetic resonance imaging: current status and future prospects. *Expert Rev Med Devices* 2006;**3**(4):427-39.
19. Kishida T, Asada H, Kubo K, Sato YT, Shin-Ya M, Imanishi J, et al. Pleiotrophic functions of Epstein-Barr virus nuclear antigen-1 (EBNA-1) and oriP differentially contribute to the efficiency of transfection/expression of exogenous gene in mammalian cells. *J Biotechnol* 2008;**133**(2):201-7.
20. Okita K, Hong H, Takahashi K, Yamanaka S. Generation of mouse-induced pluripotent stem cells with plasmid vectors. *Nat Protoc* 2010;**5**(3):418-28.
21. Seki T, Yuasa S, Fukuda K. Derivation of induced pluripotent stem cells from human peripheral circulating T cells. *Curr Protoc Stem Cell Biol* 2011 [Volume 18, Chapter 4:Unit 4 A3.1-4A3.9.].
22. Warren L, Manos PD, Ahfeldt T, Loh YH, Li H, Lau F, et al. Highly efficient reprogramming to pluripotency and directed differentiation of human cells with synthetic modified mRNA. *Cell Stem Cell* 2010;**7**(5):618-30.
23. Huang S, Kamihira M. Development of hybrid viral vectors for gene therapy. *Biotechnol Adv* 2013;**31**(2):208-23.
24. Su CH, Wu YJ, Wang HH, Yeh HI. Nonviral gene therapy targeting cardiovascular system. *Am J Physiol Heart Circ Physiol* 2012;**303**(6):H629-38.
25. Ota S, Takahashi Y, Tomitaka A, Yamada T, Kami D, Watanabe M, et al. Transfection efficiency influenced by aggregation of DNA/polyethylenimine max/magnetic nanoparticle complexes. *J Nanoparticle Res* 2013;**15**:1653-64.
26. Gao Z, Zhang L, Hu J, Sun Y. Mesenchymal stem cells: a potential targeted-delivery vehicle for anti-cancer drug, loaded nanoparticles. *Nanomedicine* 2013;**9**(2):174-84.
27. Lim J, Clements MA, Dobson J. Delivery of short interfering ribonucleic acid-complexed magnetic nanoparticles in an oscillating field occurs via caveolae-mediated endocytosis. *PLoS ONE* 2012;**7**(12):e51350.